UNIVERSIDADE FEDERAL DE SÃO CARLOS.
CENTRO DE CIÊNCIAS EXATAS E DE TECNOLOGIA.
PROGRAMA DE PÓS-GRADUAÇÃO EM ENGENHARIA QUÍMICA.

ANA ISABELA PIANOWSKI SALUSSOGLIA

AVALIAÇÃO DE MEIOS FILTRANTES COM CAMADA DE FIBRAS PRODUZIDA PELO MÉTODO DE FIAÇÃO CENTRIFUGA COM EFEITO BIOCIDA

EVALUATION OF FILTER MEDIA WITH FIBER LAYER PRODUCED BY THE CENTRIFUGAL SPINNING METHOD WITH BIOCIDAL EFFECT

SÃO CARLOS - SP
2020

ANA ISABELA PIANOWSKI SALUSSOGLIA

EVALUATION OF FILTER MEDIA WITH FIBER LAYER PRODUCED BY THE CENTRIFUGAL SPINNING METHOD WITH BIOCIDAL EFFECT

Tese apresentada ao Programa de Pós-Graduação em Engenharia Química da Universidade Federal de São Carlos, para obtenção do título de doutora em Engenharia Química.

Orientadora: Profª. Drª. Mônica Lopes Aguiar
Co-orienador: Prof. Dr. Eduardo Hiromitsu Tanabe

SÃO CARLOS - SP
2020

UNIVERSIDADE FEDERAL DE SÃO CARLOS

Centro de Ciências Exatas e de Tecnologia
Programa de Pós-Graduação em Engenharia Química

Folha de Aprovação

Assinaturas dos membros da comissão examinadora que avaliou e aprovou a Defesa de Tese de Doutorado da candidata Ana Isabela Pianowski Salussoglia, realizada em 12/03/2020:

Mônica Lopes Aguiar.

Profa. Dra. Mônica Lopes Aguiar
UFSCar

P/ Mônica Lopes Aguiar.

Prof. Dr. Eduardo Hiromitsu Tanabe
UFSM

Prof. Dr. Wanderley Pereira Oliveira
USP

Profa. Dra. Maria Angélica Martins Costa
UNESP

Vádila Giovana Guerra Béttega

Profa. Dra. Vádila Giovana Guerra Béttega
UFSCar

Prof. Dr. Clóvis Wesley Oliveira de Souza
UFSCar

Certifico que a defesa realizou-se com a participação à distância do(s) membro(s) Eduardo Hiromitsu Tanabe e, depois das arguições e deliberações realizadas, o(s) participante(s) à distância está(ao) de acordo com o conteúdo do parecer da banca examinadora redigido neste relatório de defesa.

Mônica Lopes Aguiar.

Profa. Dra. Mônica Lopes Aguiar

À minha família.

ACKNOWLEDGMENT

I thank the Graduate Program in Chemical Engineering at the Federal University of São Carlos (PPGEQ-UFSCar) and the National Council for Scientific and Technological Development (CNPq) for financial support.

RESUMO

Este estudo teve como objetivo avaliar o desempenho da filtração de ar da camada de fibras, produzida por equipamento de fiação centrífuga, aderida à superfície de um filtro comercial aplicado ao sistema de ventilação interna. Além disso, o efeito antimicrobiano do óleo essencial de tomilho adicionado à camada de fibras foi investigado para *Escherichia coli e Staphylococcus aureus*. Para esse fim, os meios filtrantes foram produzidos variando as condições de operação do equipamento, o tipo de solvente e o substrato. As características da camada de fibra (diâmetro da fibra, porosidade, tamanho do poro), o desempenho da filtração (queda de pressão, permeabilidade e eficiência de coleta de nano e micropartículas) e o efeito biocida foram analisados. Os resultados mostraram que a combinação do uso de VCS e substratos com diferentes permeabilidades levou à formação de uma camada de fibras com características diferentes; quanto mais permeável o substrato, menor a porosidade da camada de fibras formada. O aumento da potência do VCS promoveu um aumento na produção de fibras, com a diminuição do diâmetro das fibras e a porosidade da camada de fibras, consequentemente, aumento da queda de pressão; o tempo de coleta teve um forte efeito no diâmetro da fibra, no qual o maior tempo de coleta aumentou o diâmetro da fibra. A adição da camada de fibra diminuiu a permeabilidade do meio filtrante, aumentou a queda de pressão e a eficiência de coleta. A investigação do substrato coberto por fibras de PAN produzidas a partir de soluções com dimetilformamida (DMF) e dimetilsulfóxido (DMSO) indicou que os meios filtrantes DMF e DMSO apresentaram eficiência de coleta semelhantes. Isso pode indicar que o solvente DMSO promoveu uma polarização mais forte e mais consistente das cadeias PAN do que o solvente DMF, aumentando a eficiência de coleta de partículas do meio filtrante DMSO. Para este caso, esperava-se que o meio filtrante DMSO tivesse menor eficiência de coleta que o DMF porque o meio filtrante DMSO tinha um diâmetro de fibra e tamanho de poro menor que o DMF e valores próximos à porosidade da superfície. No estudo do desempenho da filtração de substrato puro e substrato coberto por fibras de PAN, foram avaliadas as eficiências de coleta de micro e nanopartículas. Houve um aumento de cerca de 20% de coleta de nanopartículas com a adição da camada de fibras de PAN. Para a eficiência de coleta de micropartículas, no início do experimento, o substrato apresentou uma eficiência de coleta de 50,5% e o substrato coberto de 71,0%. Após 30 minutos de filtração, o substrato permaneceu em filtração profunda, enquanto a adição da camada de fibra promoveu a filtração da superfície, o que aumentou significativamente a eficiência da coleta para 97,2%. Finalmente, as fibras foram fiadas nas mesmas condições de operação no substrato com óleo essencial de tomilho. O meio filtrante foi nomeado 5THY quando o óleo essencial de tomilho foi adicionado à solução de PAN e THY quando o óleo essencial de tomilho foi pulverizado no meio filtrante após a produção da camada de fibras. O meio filtrante coberto por fibras apresentou maior queda de pressão e eficiência de coleta de micro e nanopartículas e menor permeabilidade que o substrato. THY apresentou maior eficiência de coleta que o substrato e 5THY, 99% para micropartículas e 58% para nanopartículas. Através do teste antimicrobiano, verificou-se que THY apresentou uma redução de 99,999% para as bactérias *Escherichia coli* e *Staphylococcus aureus*. Para 5THY houve uma redução de 15,5 e 89,0%, respectivamente. No filtro 5THY, o óleo essencial foi adicionado às fibras antes da fiação, o que pode ter causado o aprisionamento e/ou a evaporação do óleo essencial e, portanto, diminuído a redução de bactérias.

Palavras-chave: Filtração de ar. Fiação centrifuga. Produção de fibras. Óleo essencial. Antimicrobiano.

ABSTRACT

This study aimed to evaluate the air filtration performance of the fiber layer, produced by centrifugal spinning equipment, adhered to the surface of a commercial filter media applied to the internal ventilation system. Also, to investigate the antimicrobial effect of the thyme essential oil added to the fiber layer for *Escherichia coli* and *Staphylococcus aureus*. For this purpose, filter media were produced varying the operating conditions of the equipment, the type of solvent and the substrate. The characteristics of the fiber layer (fiber diameter, porosity, pore size), filtration performance (pressure drop, permeability and collection efficiency of nano and microparticles) and the biocidal effect were analyzed. It was found that the combination of the use of VCS and substrates with different permeabilities led to the formation of a fiber layer with different characteristics; the more permeable the substrates, the lower the porosity of the formed fiber layer. The increase in the power of the VCS promoted an increase in production of fibers, with the decrease in the size of the fibers and the porosity of the fiber layer, consequently, increase in the pressure drop; the collection time had a strong effect on the fiber diameter, in which the longer collection time increased the fiber diameter. The addition of the fiber layer decreased the permeability of the filter medium, increased the pressure drop and the collection efficiency. The investigation of the substrate covered by PAN fibers produced from solutions with dimethylformamide (DMF) and dimethyl sulfoxide (DMSO) indicated that the filter media DMF and DMSO had similar collection efficiency. This may indicate that the DMSO solvent promoted stronger and more consistent polarization of the PAN chains than the DMF solvent, increasing the collection of particles from the DMSO filter medium. The DMSO filter medium was expected to have less collection efficiency than DMF because the DMSO filter medium had a smaller fiber diameter and pore size than DMF and values close to surface porosity. In the study of the filtration performance of pure substrate and substrate covered by PAN fibers, the collection efficiency of micro and nanoparticles was evaluated. For the collection efficiency of nanoparticles, the collection efficiency had an increase of about 20% with the addition of PAN fibers. For the collection efficiency of microparticles, at the beginning of the experiment, the substrate showed a collection efficiency of 50.5% and the covered substrate of 71.0%. After 30 minutes of filtration, the substrate remains in deep filtration, while the addition of the fiber layer promoted surface filtration, which significantly increased the collection efficiency to 97.2%. Finally, the fibers were spun in the same operating conditions on the substrate with essential thyme oil. The filter medium was named 5THY when the thyme essential oil was added to the PAN solution and THY when the essential oil of thyme was sprayed on the filter medium after the production of the fiber layer. The filter media covered with fibers showed a greater pressure drop and collection efficiency of micro and nanoparticles and less permeability than the substrate. THY showed higher collection efficiency than the substrate and 5THY, 99% for microparticles and 58% for nanoparticles. Through the antimicrobial test, it was found that THY showed a 99.999% reduction for the bacteria *Escherichia coli* and *Staphylococcus aureus*. While 5THY had a reduction of 15.5 and 89.0%, respectively. In the 5THY filter, the essential oil was added to the fibers before spinning, this may have caused the trapping and/or evaporation of the essential oil and, thus, reduced the reduction of bacteria.

Keywords: Air filtration. Centrifugal spinning. Fiber production. Essential oil. Antimicrobial.

LIST OF FIGURES

LIST OF TABLES

LIST OF SYMBOLS

APS	Aerodynamic particle sizer spectrometer
C_0	Particle concentration before the filter media
C_1	Particle concentration after the filter media
DMF	Dimethylformamide
DMSO	Dimethyl sulfoxide
E	Collection efficiency
FS	Forcespinning
k	Permeability constant
L	Thickness of the filter media
NaCl	Sodium chloride
PAN	Polyacrylonitrile
PBS	Phosphate-buffered saline
PCA	Plate count agar
Q_f	Quality factor
SEM	Scanning electron microscopy
SMPS	Scanning mobility particle size
THY	Fiber covered filter medium produced from the solution of 10 wt. % PAN with thyme essential sprayed
t=0	At the beginning of the test
t=30	30 minutes of the start of the test
VCS	Vacuum collection system
v_L	Face velocity
26G½"	26-gauge half-inch needles
30G½"	30-gauge half-inch needles
5THY	Fiber covered filter medium produced from the solution of 10 wt. % PAN and 5 wt. % thyme essential oil
ΔP	Pressure drop
μ	Fluid viscosity

SUMMARY

INTRODUCTION

In recent decades there has been a growing concern about comfort, health, and well-being indoor (Cincinelli and Martellini, 2017). Many health problems have been associated with air pollution, for that, the concern of air quality has been increasing (World Health Organization, 2017). People spend about 80 - 90% of the day in the enclosed environments (Klepeis *et al.*, 2001). Bioaerosols have become a preoccupation in indoor air quality and contribute up to 34% of indoor air pollution (Mandal and Brandl, 2011). Bioaerosols are in the environment and include pollen, bacteria, fungi, viruses, plant or animal debris. Airborne bioaerosols generally range in size from 1.0 to 5.0 μm (Ghosh, Lal, and Srivastava, 2015). Exposure to bioaerosols has been linked to several health problems as diseases in the respiratory tract and eyes, asthma, rhinitis, bronchitis, rashes on the skin, cancer, diarrhea, headache, hypersensitivity pneumonitis (Douwes *et al.*, 2003; Menetrez *et al.*, 2009).

Filtration is one of the most common methods for air purification due to its simple structure and low cost (Donovan, 1985). However, the filter media not provide sufficient protection against pathogenic bioaerosols, mainly if the captured microorganisms are re-entrained into the air. Besides, some filter media may be colonized by bacteria and fungi (Maus, Goppelsröder and Umhauer, 2001; Noris, Siegel and Kinney, 2011). Therefore, an alternative is modifying the filter media to combat the microorganisms. Manufacture filter media impregnated with an antimicrobial agent have been a possibility.

Recent studies reported antimicrobial agents have been incorporated into spun fibers that covered the filter media (Bortolassi *et al.*, 2019; Hwan *et al.*, 2015; Zhu *et al.*, 2018). Some antimicrobial agents commonly used for filtration applications are silver (Lala *et al.*, 2007), chitosan (Desai *et al.*, 2009), fiberglass-acrylic (Cecchini *et al.*, 2004). Besides antimicrobial agents incorporated into spun fibers inactivated the microorganisms, the addition of the spun fiber layer into filter media improves filtration performance because the characteristics of the fiber layer such as high surface area, small fiber diameter, and excellent mechanical performance are extremely favorable in air filtration application (Leung, Hau and Choy, 2018; Li *et al.*, 2013; Liu *et al.*, 2015).

The centrifugal spinning technique has been highlighted among the various methods of spun fiber production. This technique could use a wide range of materials, and high-concentration solutions, no dependent on solution conductivity, having high productivity, low costs, large-scale production, eco-friendly process, and equipment easy to implement (Lu *et al.*, 2013; Padron *et al.*, 2013; Sarkar *et al.*, 2010). Therefore, many factors influence the spun fiber formation by centrifugal spinning equipment such as operational parameters, equipment components, material properties, and environment (Padron *et al.*, 2013; Sarkar *et al.*, 2010). Recent studies have described fiber production by centrifugal spinning equipment (Fang *et al.*, 2016; O'Haire *et al.*, 2013; Padron *et al.*, 2013), few applications have been reported as anodes for lithium-ion batteries (Agubra *et al.*, 2016), uranium adsorption (Rostamian, Firouzzare, and Irandoust, 2019), and wound dressing (Xu *et al.*, 2014), but no study applied to air filtration.

In the last decades, the use of substances derived from plants and animals due to the many biomedical properties was observed. The essential oils, that are generally produced from the steam distillation of plants, have been used to combat bacteria, fungi, and viruses (Hammer, Carson and Riley, 1999). Some applications of the essential oils as an antimicrobial agent are biofilm (Kavanaugh and Ribbeck, 2012), food application (Gutierrez, Barry-Ryan and Bourke, 2008; Sallam, Ishioroshi and Samejima, 2004), wound dressing (Liakos *et al.*, 2014), and medicine (Vuuren, Van, Suliman and Viljoen, 2009), for example.

Research has recently reported the incorporation of the essential oil into spun fibers. Balasubramanian and Kodam (2014) spun polyacrylonitrile (PAN) and lavender oil nanofiber with the halo of inhibition unchanged for 30 days for *Staphylococcus aureus* and *Klebsiella pneumoniae* bacteria. Zhang *et al.* (2017) investigated the mechanical and antimicrobial properties of polylactic acid fibers containing *Melaleuca alternifolia* and *Leptospermum scoparium* essential oil. The fiber modified produced halo of inhibition for *Staphylococcus epidermidis*. There are some studies about natural antimicrobial agents used for filtration application, as, *Sophora flavescens* (Choi *et al.*, 2015), propolis and grapefruit seed extracts (Woo *et al.*, 2015), but, no information about the

addition of essential oils for this propose. Thus, the addition of essential oil to the fiber covered filter medium can be a promising choice as an antimicrobial agent.

Thyme (Niu *et al.*, 2016), cumin (Alizadeh Behbahani, Noshad and Falah, 2019), oregano (Zhou *et al.*, 2018), ginger (Silva *et al.*, 2018), cinnamon (Jiang *et al.*, 2019), clove (Radünz *et al.*, 2019), garlic, and onion (Benkeblia, 2004) are some essential oil with antimicrobial activity. Thyme essential oil has stood out as an antimicrobial and antifungal agent in the food industry as active packaging against *Campylobacter jejuni* in chicken (Lin, Zhu and Cui, 2018), a natural preservative in bakery product (Gonçalves *et al.*, 2017) and film for fruit preservation (Lian *et al.*, 2020), in antimicrobial protection of natural textiles (Walentowska and Foksowicz-Flaczyk, 2013) and combination with conventional antimicrobials (Vuuren, Van, Suliman and Viljoen, 2009), for example.

Therefore, this study aimed to investigate the characteristic of the fiber layer produced by centrifugal spinning varying the operational conditions of the equipment, solvent and substrate type, and filtration performance of the spun fiber covered filter media. Besides, this study quantitatively evaluated the antimicrobial effect of essential oil of thyme added to the filter media covered by spun fiber for the bacteria *Escherichia coli* and *Staphylococcus aureus*. This was studied in chapters, containing introduction, materials and methods, results and discussions, and conclusion. Chapter 1 addresses the literature review on filtration, filter media covered with fiber and essential oil. Chapter 2 evaluated the filtration performance of PAN fibers covered filter media and characteristics of the fibers layer produced under different operational conditions (needle diameter, rotation speed, collection time, and vacuum collection system power) and substrate types. Then, in Chapter 3, it was evaluated the filtration performance of fibers covered filter media and the characterization of the fiber layer produced under the same operational condition using PAN solution produced by dimethylformamide (DMF) and dimethyl sulfoxide (DMSO) solvents. In Chapter 4, a filter media with low filtration performance was covered by PAN fibers and the filtration performance was evaluated at the beginning and 30 minutes after the start of the test for micro and nanoparticles. In Chapter 5,

the antimicrobial effect of some essential oils was evaluated, the thyme essential oil was added to filter media after and before the spinning process to evaluate the antimicrobial effect, and the filtration performance of fiber covered filter media was evaluated for micro and nanoparticles.

1. LITERATURE REVIEW

1.1. FILTRATION

Filtration is one of the most used techniques to capture particles from the gas stream, due to its high efficiency, simplicity of operation, flexibility, and economy. The particles are captured as they travel through the filter body. The collection occurs due to the physical contact between the particles and the collecting element, requiring the adhesion of the particles (Donovan, 1985). Two parameters are used to determine filtration performance: collection efficiency and pressure drop. Higher total collection efficiency with lower pressure drop during operation is expected. Such parameters are limited by the speed of the gas surface (Dullien, 1989).

Filtration is classified depending on the filter region in which the particles are collected. In deep filtration, particles are captured as they enter the filter structure, also known as internal filtration. Filtration is classified as surface filtration when a layer of particles is formed on the filter surface, known as a filter cake. In this stage, the filter cake becomes responsible for the capture of particles (Dullien, 1989). In the surface filtration stage, the filter acts only as a support for the filter cake, which can remove smaller particles from the gas stream. Therefore, it is interesting to establish the stage of superficial filtration as soon as possible so that the system reaches greater collection efficiency (Rothwell, 1980). There is also a transition phase between internal and surface filtration. This phase is characterized by the formation of dendrites. Dendrites are agglomerations of particles that start to act as new particle collectors.

The filtration efficiency depends most of the time on the selection of the filter medium that requires a consideration of the advantages and disadvantages of each type of filter.

1.1.1. **Collection mechanism**

The collection of particles in a filter medium is done initially through the fibers. The mechanisms that govern this capture are diffusional, inertial, direct interception, gravitational, and electrostatic attraction, as can be seen in Figure 1.

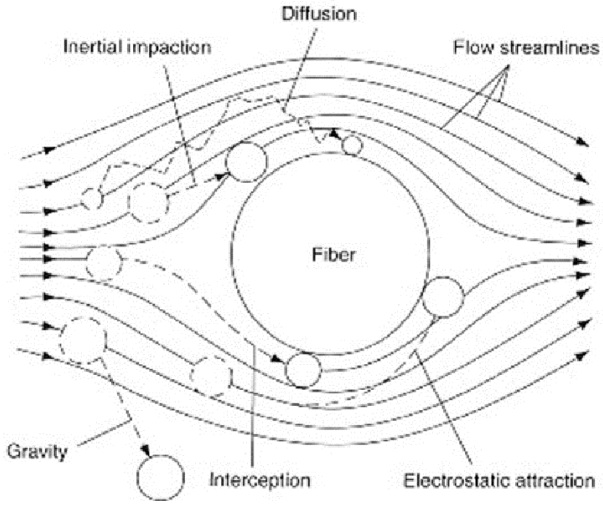

Figure 1. Collection mechanism (Senthil and Punitha, 2017).

The transport of particles in a fluid is strongly linked to the interactions that take place between the gas molecules and the particles present in it. The Knudsen number is dimensionless that characterizes the behavior of the particle concerning gas, the particle size influencing the behavior of the aerosol and the laws that determine its properties. The Knudsen number (K_n), represented by Equation 1 (Hinds, 1999):

$$K_n = \frac{2\,\lambda}{d_p} \quad (1)$$

where the ratio between the average free path of the molecules in the gas (λ) and the diameter of the particles (d_p).

The average free path of the molecules in the gas is defined as the distance that a molecule of the gas travels before it collides with another. If the fluid is air, the average free path can be determined by Equation 2:

$$\lambda = 2.15\ 10^{-4} \mu\ P\ T^{0.5} \quad (2)$$

where μ the air viscosity, P is the pressure and T the absolute temperature.

The behavior of the particle concerning gas is characterized by the Knudsen number since the particle size influences the behavior of the aerosol and the laws that determine its properties (Hinds, 1999). Therefore, in the case of particles with reduced diameters, in such a way that they present sizes of the same order of magnitude as the average free path of the molecules (K_n >> 1),

such particles do not see the gaseous medium as a continuous mass but as a cluster of particles. On the other hand, if the particle is larger than the average free path (K_n << 1), it will see the gas as a continuous medium.

In the case of the continuous flow hypothesis, the correction of the effect of interactions at the molecular level, when the particles flowing in the fluid are small, can be done by the Cunningham slip factor (F_s) Equation 3 (Clift, Grace and Weber, 1978):

$$F_s = 1 + K_n \left[1.246 + 0.42\ exp\left(\frac{-0.87}{K_n}\right)\right] \quad (3)$$

The Cunningham slip factor takes into account the non-continuity of the medium for particles that have a size close to the average free path. Thus, from these concepts defined to understand the interaction between the gas and the constituent particles, it becomes simpler to present the description of each collection mechanism, which are idealized representations of the physical phenomena that promote particle-fiber contact.

1.1.1.1. Diffusional mechanism

The diffusional mechanism results from the random (Brownian) movement to which small particles are subjected in a gas, known as Brownian diffusion (Coury, 1983). This mechanism occurs, predominantly, in submicron particles and at low filtration speeds.

The small particles do not follow the airflow lines perfectly due to their displacement by the constant collisions of air molecules. Therefore, such particles diffuse in several directions, greatly increasing the likelihood that they will hit the fibers and remain there. By reducing the speed of the gas, efficiency tends to increase, as the residence time in the filter medium is longer.

In the case of very small particles, the current lines do not coincide with the trajectory of the particles, which is due to the random movement of the particles. This collection mechanism is especially active for particles with diameters smaller than 1 μm submitted to low filtration speeds (Dullien, 1989)**.**

The collection efficiency due to the diffusional mechanism (η_d) of each fiber individually can be obtained by Equation 4 (Lee and Liu, 1982)**:**

$$\eta_d = 2.6 \left(\frac{\varepsilon}{Ku}\right)^{1/3} Pe^{-2/3} \quad (4)$$

where Ku is the hydrodynamic coefficient of Kuwabara and Pe is the number of Peclet, given by equations 5 and 6, respectively:

$$Ku = \frac{-\ln(1-\varepsilon)}{2} - \frac{3}{4} + (1-\varepsilon) - \frac{(1-\varepsilon)^2}{4} \quad (5)$$

$$Pe = \frac{U_o D_f}{D} \quad (6)$$

where D is the diffusivity coefficient, for spherical diameter particles, and can be obtained by Equation 7:

$$D = \frac{K_B T F_s}{3\pi\mu d_p} \quad (7)$$

where K_B is the Boltzman constant, T is the absolute temperature, μ is the fluid viscosity and F_s is the Cunningham slip factor.

1.1.1.2. Inertial mechanism

The collection by the inertial mechanism occurs due to the inertia of the particles. The higher the kinetic energy of the particles, the greater the collection efficiency by this mechanism, therefore, this mechanism predominates at high gas speeds. The collection occurs because the particles cannot follow the gas stream (Hinds, 1999). If the curvature of the gas streams is high enough and the mass of the particle too, there is a high probability that the particle will hit the collector and then return to the gas stream by elastic shock. This is probably one of the reasons that explain the discrepant data found in the literature for the efficiency of inertial collection.

The Stokes number is the parameter that describes the inertial mechanism for collecting particles in filter media (Willeke and Baron, 1993). High Stokes numbers reflect a high probability of collection by this mechanism, while low Stokes numbers reflect a low probability of collection. The number of Strokes (S_t) is determined by Equation 8:

$$S_t = \frac{F_s d_p^2 \rho_p U_o}{18\,\mu\, D_f} \quad (8)$$

where ρ_p and d_p are particle density and diameter, respectively.

Friedlander and Pasceri (1965) proposed Equation 9, to determine the filtration efficiency of the particles by the inertial mechanism (η_i):

$$\eta_i = 0.0075\ {S_t}^{6/5} \tag{9}$$

1.1.1.3. Interception mechanism

The direct interception results from the ratio of the relative size between the particle and the collector ($R = d_p/D_f$). This mechanism is significant with a particle diameter of the order of magnitude slightly below the diameter of the collector (Coury, 1983). The particles follow the gas current lines and can be captured when its center passes at a distance less than or equal to their radius from the surface of the collector.

Lee and Liu (1982) proposed Equation 10 for the collection efficiency by the direct interception mechanism (η_{id}):

$$\eta_{id} = 0.6\frac{\varepsilon}{K}\left(\frac{R^2}{1+R}\right) \tag{10}$$

According to Liu and Rubow (1990)**,** the slipping effect of the gas must be taken into account when describing the flow around the fiber in cases where the fiber diameter is the same order of magnitude as the average free path of the gas molecules. About this effect, these same authors proposed the addition of a correction factor (C_r) in the collection efficiency equation of the direct interception mechanism proposed by Lee and Liu (1982). The expression proposed by Lee and Liu (1982) together with the correction factor suggested by Liu and Rubow (1990) is represented in Equation 11 and 12, respectively:

$$\eta_{id} = 0.6\frac{\varepsilon}{K}\left(\frac{R^2}{1+R}\right) C_r \tag{11}$$

$$C_r = 1 + \frac{1.996\ K_n}{R} \tag{12}$$

1.1.1.4. Gravitational mechanism

The gravitational mechanism acts to collect it because it causes a deviation in its normal path, due to the effect of gravity on the particle. It is predominant for low gas speeds and large particles. The collection efficiency depends on the direction of the flow and the direction of the gas stream since in a flow from top to bottom there is a tendency for particles to approach the collector (Coury, 1983).

The collection efficiency described by the gravitational mechanism (η_g) be estimated by Equation 13 (Tien and Ramarao, 2007):

$$\eta_g = \frac{(1-\varepsilon)^{2/3} V_t}{U_o} \tag{13}$$

where V_t is the terminal velocity of the particle and can be determined by Equation 14:

$$V_t = \frac{d_p^2 g \rho_p}{18\mu} \tag{14}$$

where g is the acceleration due to gravity.

1.1.1.5. Electrostatic attraction mechanism

The collection by the mechanism may be due to the presence of electrostatic charges in the particles and the filtering medium, or it may be induced by an external electric field. The attraction between particle and collector occurs through several mechanisms, identified by Ranz and Wong (1952): the attraction between charged particle and collector with opposite charge (Coulômbica force), the attraction between the charged particle and its dipole-image in the collector, attraction between the charged particle and its dipole-image in the particle, repulsion of a charged particle by a neighboring particle with similar charge, and attraction between the charged particle and grounded collector, with opposite charge induced by neighboring particles.

According to Coury (1983), the collection efficiency by the electrophoretic mechanism (η_e) from the charged particle with charge q is given by Equation 15:

$$\eta_e = 8.242 K_M^{0.494} \quad (15)$$

is valid for S_t < 10^{-3} and 10^{-4} < K_M< 10^{-6}, and the expression for K_M can be seen in Equation 16:

$$K_M = \frac{\gamma_c F_s q^2}{3\pi^2 \varepsilon_o d_p D_f^2 \mu U_o} \quad (16)$$

where ε_o the vacuum permittivity is 8.85510^{-12} A.s/V.m, q the particle charge and γ_c is the collector's polarization coefficient, given by Equation 17:

$$\gamma_c = \frac{\varepsilon_c - \varepsilon_f}{\varepsilon_c + 2\varepsilon_f} \quad (17)$$

where ε_c is the particle dielectric constant and ε_f is the fluid dielectric constant.

1.1.1.6. Simultaneous collection by several mechanisms

The total collection efficiency of a collector is generally associated with the sum of the individual efficiencies of each collection mechanism in Equation 18:

$$\eta_t = \eta_d + \eta_i + \eta_{id} + \eta_g + \eta_e \quad (18)$$

1.2. FIBER COVERED FILTER MEDIA

The filter media containing nanofibers generally have a double layer in which the fiber layer is deposited on the substrate. The fiber layer can be spun by different techniques, the most common of which are electrospinning (Deitzel *et al.*, 2001), pressurized gyration (Mahalingam and Edirisinghe, 2013), melt blowing (Ward, 2005), solution blow spinning (Medeiros *et al.*, 2009), and centrifugal spinning (Sarkar *et al.*, 2010).

The substrates are selected to provide adequate mechanical properties and complementary functionalities to the fiber layer while it improves the filtration performance. The substrates are selected because they have pleating properties, facilitate the fabrication of the filter media, and improve durability in use and cleaning (Grafe and Graham, 2003). Among the various types of substrates, the most common are cellulose, fiberglass, polyester, and nylon. Besides, Nicosia *et al.* (2016) reported that the arrangement of the fiber layer is influenced by the morphology of the substrate.

The addition of the fiber layer improves the filtration performance. This is because the characteristics of spun fibers as high surface area, small fiber diameter, and small pore size, are favorable in air filtration applications. Filter media with fiber layers have been the focus of several recent studies (Huang *et al.*, 2003; Leung, Hau e Choy, 2018; Li *et al.*, 2013; Liu *et al.*, 2015). A decrease in the porosity of the fiber layer has been linked to increasing the collection efficiency and the pressure drop (Wang, Kim, and Pui, 2008). Smaller average fiber diameter can significantly improve the collection efficiency (Balgis *et al.*, 2015; Yun *et al.*, 2010), although the influence of the fiber diameter distribution also has to be taken into account (Payen *et al.*, 2012; Zhang, Shim, and Kim, 2009).

1.2.1. **Centrifugal spinning**

The centrifugal spinning is composed of the spinneret and the collector, as can be seen in Figure 2. The centrifugal spinning manufacturing micro and nanofibers of polymers, from solutions or melts, metallic, ceramic or composites (Sarkar *et al.*, 2010). The solution is put in the spinneret and it flows through the needles to form the fibers by the centrifugal force action. At the needle exit, the diameter of the solution jet is reduced well below the needle diameter due to the angular velocity. The jet continues to be elongated during its trajectory around the spinneret (the most reduction of the fiber diameter happens in this period). Then, the fibers are gathered on the collection method (Padron *et al.*, 2013).

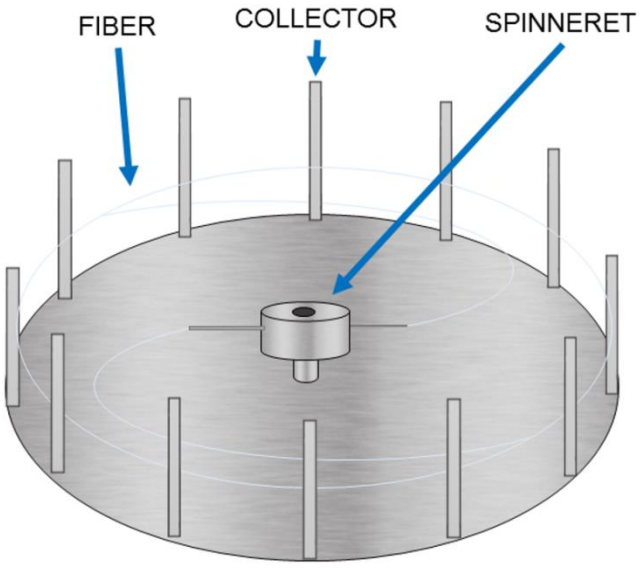

Figure 2. Schematic illustration of centrifugal spinning.

The centrifugal spinning technique has stood out for increasing the choice of material, equipment flexible, easy to implement, fiber formation is no dependent on solution conductivity, dispense with the use of an electric field, lower fiber cost, large-scale production, and the fiber can be produced with high concentration solution (Sarkar *et al.*, 2010). Some applications of this technique are wound dressing (Xu *et al.*, 2014), pharmaceutical application (Akia *et al.*, 2019; Mamidi *et al.*, 2019), batteries (Agubra *et al.*, 2016; Flores *et al.*, 2018), adsorption (Kummer *et al.*, 2018), filter medium (Missau *et al.*, 2018; Salussoglia, Tanabe and Aguiar, 2019), the colorimetric sensor for food (Valdez *et al.*, 2019), fibrous color dosimeter (Kinashi *et al.*, 2018), and tissue engineering (Lukášová *et al.*, 2019; Mamidi *et al.*, 2019).

1.2.1.1. Fiber production

The fiber production is affected of different parameters as equipment components, material properties (viscosity, elasticity, surface tension, rate of solvent evaporation), and operational parameters (solution concentration, rotational speed, needle diameter, needle-collector distance, temperature) (Lu *et al.*, 2013; Padron *et al.*, 2013; Sarkar *et al.*, 2010).

Lu *et al.* (2013) researched the PAN fiber produced by centrifugal spinning varying the operational parameters (solution concentration, rotational speed, needle diameter, and needle-collector distance) and their effects on the fiber morphology.

1.2.1.1.1. *Solution concentration*

The formation of the fiber is influenced by the concentration of the polymer. The ideal concentration of the solution resulting in fine fibers due to the increased probability of entanglement of the polymeric chain and resisting the formation of the bead. The fiber diameters of PAN fibers increased from 406, 458, 440, 665, to 1077 nm when solution concentration from 10, 12, 13, 14, to 15 wt.%, respectively. The increase in solution concentration and viscosity leads to larger fiber diameter because highly-viscous solution often exhibits longer stress relaxation time, which limits the evaporation of solvents and resists jet fracturing, elongation and thinning (Lu *et al.*, 2013).

1.2.1.1.2. *Rotational speed*

The centrifugal force experienced by the liquid jets increases with the increasing rotation speed. Higher centrifugal force can induce greater extension and thinning of the polymer jets, which results in thinner fiber diameters. The fiber diameter was 663, 541, 440 nm with the rotational speed 2000, 3000, 4000 rpm, respectively. The rotational speed increased when the centrifugal force exerted on the solution per volume increased significantly while the surface tension remained the same. Thus, when rotational speed was increased fiber diameter reduced (Lu *et al.*, 2013).

1.2.1.1.3. *Needle diameter*

Smaller needle diameter typically decreases the mass throughput, that turn restricts the fiber diameter. The needle diameters of 0.4, 0.8, and 1.0 mm decreased the fiber diameter from 895, 807, 665 nm, respectively. Therefore, It is suggested that to fabricate thinner fibers smaller needle diameter be used. (Lu *et al.*, 2013; Zhang and Lu, 2014).

1.2.1.1.4. *Needle-collector distance*

Changing the needle-collector distance affects the fiber morphology because modify the flight time of the solution jet. There is a minimum needle-collector distance that allows the adequate evaporation of the solvent before arriving at the collector. as longer needle-collector distance longer distance traveled through the solution jet, which promoted the formation of smaller fiber diameter. The fiber diameter decreased from 665, 658 to 647 nm when the needle-collector distance increased from 10, 20 to 30 cm, respectively. The average fiber diameter little changed when the needle-collector distance increased (Lu *et al.*, 2013; Zhang e Lu, 2014).

1.3. ESSENTIAL OIL

Egypt, China, and India civilizations have used essential oil as a popular complementary from at least 6000 years (Alok, Rakesh and Sushil, 2000). The global market value of herbal products is approximately US$ 62 billion, and growth of up to 5 trillion is expected by 2050 (Bhattacharya, Reddy and Mishra, 2014). The industries of cosmetics, food, perfume, and pharmaceutical based on essential oil or chemicals with a natural aroma and more than 250 types of

essential oils are traded annually in the amount of US$ 1.2 billion (Akthar, Degaga and Azam, 2014). Essential oil is defined by the International Organization for Standardization (ISO/D1S9235.2) as a product produced by distillation with water, steam, mechanical processing or dry distillation of natural materials.

The inhibitory effect of essential oils has been attributed to the presence of the aromatic nucleus containing a polar functional group (Farag *et al.*, 1989). Much essential oil with antimicrobial effect were reported in the literature as thyme (Niu *et al.*, 2016), rosemary (Jiang *et al.*, 2011), cumin (Alizadeh Behbahani, Noshad and Falah, 2019), oregano (Zhou *et al.*, 2018), ginger (Silva *et al.*, 2018), cinnamon (Jiang *et al.*, 2019), clove (Radünz *et al.*, 2019), garlic and onion (Benkeblia, 2004). Essential oils are used in aromatherapy and in the treatment of various diseases, including antifungal, antiviral, anti-inflammatory, anti-tumor, spasmodic, hormonal, and antimicrobial actions (Ali *et al.*, 2015). Essential oil has been used as an antimicrobial effect for many purposes such as biofilm (Kavanaugh and Ribbeck, 2012), food application (Gutierrez, Barry-Ryan and Bourke, 2008; Sallam, Ishioroshi and Samejima, 2004), wound dressing (Liakos *et al.*, 2014), and medicine (Vuuren, Van, Suliman and Viljoen, 2009).

1.3.1. **Thyme essential oil**

Thyme oil containing around 42.7% of thymol and 36.0% of p-cymene as the most prevalent compounds. The presence of phenolic OH groups promotes the higher inhibitory action of thymol because the OH group is quite reactive and easily forms hydrogen bonds with active sites of enzymes. Besides the aromaticity of the molecule, the inductive effect of the isopropyl group must also be taken into account (Farag *et al.*, 1989). Khan, Shafee and Asif (2017) evaluated the halo of inhibition of Pakistani variety of the thyme essential oil and obtained 31 mm for Escherichia coli and 25 mm for Staphylococcus. Walentowska and Foksowicz-Flaczyk (2013) reported the antimicrobial effect of the halo of inhibition test for 8% of thyme essential oil added to the protection of natural textiles. No count for *Corynebacterium xerosis*, *Micrococcus luteus*, and *Staphyloccocus haemolyticus* was found and the halo of inhibition exceeded 5

mm for *Bacillus licheniformis*, *Staphyloccocus aureus*, *Escherichia coli*, *Klebsiella pneumoniae*, and *Pseudomonas aeruginosa*.

1.3.2. **The essential oil in spun fiber**

In recent studies the essential oil has been incorporated into spun fibers. Mori *et al.* (2015) investigated the effect of inclusion of candeia essential oil on the properties of the polylactic acid (PLA) layer obtained by electrospinning. The addition of essential oil decreased the melting temperature of the fibers and the glass transition, and increased the fiber diameter, indicating that the plasticizing effect of essential oil in the PLA matrix. No differences in fiber crystallization was showed by x-ray diffraction. Rieger and Schiffman (2014) added cinnamaldehyde in chitosan/poly(ethylene oxide) solution and spun into mats by electrospinning. The cinnamaldehyde promoted high inactivation rates against *Escherichia coli* and *Pseudomonas aeruginosa*. Balasubramanian and Kodam (2014) spun PAN-lavender oil nanofibers produced by electrospinning. The antibacterial activity was evaluated against *Staphylococcus aureus* and *Klebsiella pneumoniae*. PAN nanofibers had antimicrobial properties from 14 to 15 mm of inhibition zone in at least 8 hours, and unchanged for 30 days. Zhang *et al.* (2017) investigated mechanical and antimicrobial properties of polylactic acid (PLA) fibers containing Melaleuca alternifolia and Leptospermum scoparium essential oil. The essential oils acted as plasticizers for PLA, lowering the glass transition temperature of the resulting composite fibers. The fiber produced halo of inhibition for *Staphylococcus epidermidis*. Thus, the essential oils have been used as an antimicrobial agent for various applications and have been successfully added to the spun fiber.

2. EVALUATION OF A VACUUM COLLECTION SYSTEM IN THE PREPARATION OF PAN FIBERS BY FORCESPINNING FOR APPLICATION IN ULTRAFINE PARTICLE FILTRATION

2.1. INTRODUCTION

Ultrafine particles, which are particles with a diameter smaller than 100 nm, contribute around 90% of the atmospheric particle concentration in urban areas (Choi and Kim, 2018). Particles with these dimensions have been linked to health problems such as lung cancer, stroke, heart diseases, and premature death (World Health Organization, 2017). Capturing these particles is a major challenge, due to their small size.

Filtration is one of the commonest and most efficient methods of gas-solid separation. The future market for fabric filter systems is estimated to be worth US$ 16.34 billion in 2025 (Maduna and Patnaik, 2017). The filter medium selection is of fundamental importance and should prioritize high collection efficiency, low pressure drop and operating cost. These properties are directly related to porosity, permeability constant, fiber diameter, and media thickness. The most used filter media for collecting micro particles from the gas stream are fibrous, due to their high collection efficiency, production simplicity, and low cost. The fibrous filter medium has a large range of fibers sizes positioned preferably perpendicular to the direction of fluid flow. The fibrous filter is commonly made of cellulose, glass, quartz, and polymers (Willeke and Baron, 1993).

Thus, spun ultra-fine fibers, which are applied in areas as diverse as tissue engineering (Perez-Puyana *et al.*, 2019), pharmaceuticals (Hobzova *et al.*, 2019), sensors (Chang *et al.*, 2019), food production (Niu *et al.*, 2018), have received increasing attention in air filtration (Gopal *et al.*, 2006; Yin *et al.*, 2013). This is because the characteristics of spun ultra-fine fibers, such as high surface area, small fiber diameter, and excellent mechanical performance, are extremely favorable in air filtration applications and have been the focus of several recent studies (Huang *et al.*, 2003; Leung, Hau and Choy, 2018; Li *et al.*, 2013; Liu *et al.*, 2015; Sambaer, Zatloukal and Kimmer, 2011). High surface-to-volume ratios and small pore sizes provide spun media with good

performance in air filtration (Deitzel *et al.*, 2001; Gibson, Schreuder-Gibson and Rivin, 2001), while the arrangement of the fiber layer is influenced by the morphology of the substrate (Nicosia *et al.*, 2016). A decrease in the porosity of the fiber layer has been found to increase the collection efficiency, as well as the pressure drop (Wang, Kim and Pui, 2008). Smaller average fiber diameter can significantly improve the collection efficiency (Balgis *et al.*, 2015; Yun *et al.*, 2010), although the influence of the fiber diameter distribution also has to be taken into account (Payen *et al.*, 2012; Zhang, Shim and Kim, 2009). However, these filter media have a high cost.

To improve the performance of the filter media with a layer of polymeric spun ultra-fine fiber as well as to reduce the operation and maintenance costs of air filters it is necessary to understand the formation and production of the spun fibers. The commonest methods of ultra-fine fiber production include electrospinning (Deitzel *et al.*, 2001), pressurized gyration (Mahalingam and Edirisinghe, 2013), melt blowing (Ward, 2005), solution blow spinning (Medeiros *et al.*, 2009), and Forcespinning™ (FS) (Sarkar *et al.*, 2010). FS is a promising method of producing micro and nanoscale polymeric fibers from polymer solutions or melts, using centrifugal forces. The FS fiber production allows the use of a wide range of materials with high productivity, low costs, and large-scale production. No dependent on solution conductivity, no electric field is needed, high-concentration solutions can be used, besides being an eco-friendly process, and equipment simple to implement (Lu *et al.*, 2013; Padron *et al.*, 2013; Sarkar *et al.*, 2010). The fiber production starts with the addition of a solution or melt polymer in the spinneret. After, the solution flows through the needles because of the centrifugal forces. The solution jet in contact with the air is elongate and finally, the fibers are deposited in the collector (Padron *et al.*, 2013). Many factors influence the fiber formation such as operational parameters, equipment components, material properties, and environment (Padron *et al.*, 2013; Sarkar *et al.*, 2010). Several recent studies have described fiber production by centrifugal force methods (Fang *et al.*, 2016; O'Haire *et al.*, 2013; Padron *et al.*, 2013), but few applications have been reported as anodes for lithium-ion batteries (Agubra *et al.*, 2016), uranium adsorption (Rostamian, Firouzzare and Irandoust, 2019), and wound dressing (Xu *et al.*, 2014). Lu *et al*.

(2013) evaluated polyacrylonitrile (PAN) fiber production by this technique, using a standard collection system (Lu *et al.*, 2013). This study shows that the operational parameters change the morphology of the fibers, especially the fiber diameter.

The collector is one of the equipment components that affect fiber formation (Sarkar *et al.*, 2010). A collector option is the vacuum collection system (VCS) which is a box that produces reverse airflow. The filter medium (substrate) is fixed on the VCS, after that the fibers are spun over the filter medium under reverse airflow action. Certainly, the airflow will cause changes in fiber production. However, there is little information available concerning the use of VCS in the production of spun fibers. This collector was used to producing nylon 6 fiber (Krifa and Yuan, 2015) and in the application of the purification of crude wax (Missau *et al.*, 2018).

Therefore, the aim of this paper was to produce a systematic evaluation of the PAN fibers production using a Forcespinning system equipped with a vacuum collection system, as well as to evaluate the filter media with spun fiber layer in the air filtration of nanoparticles. Furthermore, the effects of the filter media type used as a substrate and the operational parameters of centrifugal spinning (collection time, VCS power, needle diameter, and rotation speed) were investigated for filtration performance and characteristics of the fiber layer.

2.2. EXPERIMENTAL

2.2.1. **Materials**

Polyacrylonitrile (PAN, Mw: 150,000 g/mol) and N, N-dimethylformamide (DMF, anhydrous, 99.8%), purchased from Sigma-Aldrich, were used to produce the fibers. Five different filter media were used as substrates (denoted S1, S2, S3, S4, and S5). Sodium chloride (NaCl, 99%) was used to generate particles, purchased from Sigma Aldrich.

2.2.2. **Preparation of the fibers**

FS is composed of the spinneret and a collector, the vacuum collection system (VCS) was selected as a collector, as shown in Figure 3 a. Metal bars were used to facilitate the cleaning of the equipment. The substrate, measuring

21 x 5 cm, was fixed to the VCS at 5 cm from the side edges and 7.5 cm from the bottom edge, as can be seen in Figure 3 b. The fibers were prepared from a solution of 12 wt. % PAN dissolved in DMF by heating (60 °C) and stirring. The solution was put in the spinneret and dripped down the needles through centrifugal forces. The solution jet was elongated in contact with air and finally was deposited on the substrate (filter media) under the influence of reverse airflow promoted by VCS.

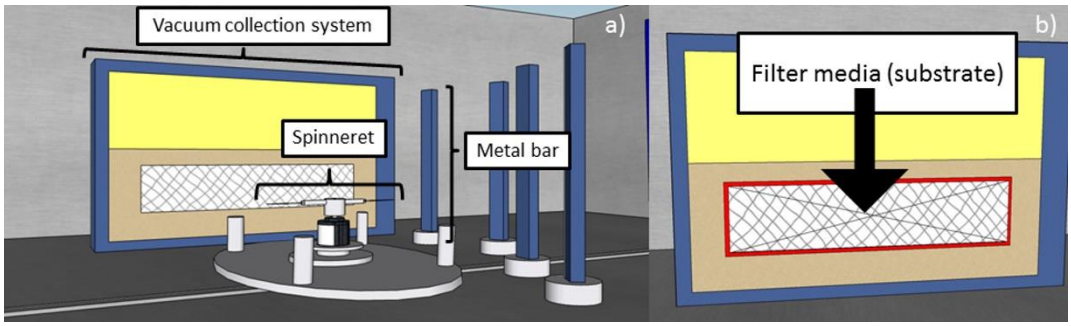

Figure 3. Schematic illustration of the FS system: (a) arrangement of FS components; (b) vacuum collection system.

The fibers were spun over all the substrates (S1-S5) under the same operational conditions, using 26-gauge half-inch needles (26G½"), 10 cm needle-collector distance, 4000 rpm rotation speed, 60 s collection time, and 100% VCS power. The effect of the substrate type on the characteristics of the fiber layer and the filtration performance was evaluated using these fixed operational conditions. After the fibers were spun on the substrates, S1-S5 was named M1-M5.

The fibers were spun over S4 for evaluate of the effects of collection time (60 and 180 s), VCS power (25 to 100%), needle diameter (26G½ "and 30G½"), and rotation speed (4000 and 6000 rpm) individually, maintaining the other parameters on initial conditions. The filter media M4 was used as a reference and each filter medium has been named according to the changed operating condition. The filter media obtained after coating with the fibers were named according to the substrate type and the operational conditions, as shown in Table 1.

Table 1. Filter media listed according to substrate type, collection time, VCS power, rotation speed, and needle size.

Filter media	Substrate	Rotation speed (rpm)	Needle size	Collection time (s)	VCS power (%)
M1	**S1**	4000	26G½"	60	100
M2	**S2**	4000	26G½"	60	100
M3	**S3**	4000	26G½"	60	100
M4	**S4**	4000	26G½"	60	100
M5	**S5**	4000	26G½"	60	100
T180	S4	4000	26G½"	**180**	100
VCS25	S4	4000	26G½"	60	**25**
VCS50	S4	4000	26G½"	60	**50**
VCS75	S4	4000	26G½"	60	**75**
V6000	S4	**6000**	26G½"	60	100
N30	S4	4000	**30G½"**	60	100

2.2.3. **Fiber layer characterization**

The fiber layers were characterized by an analysis of images, images with 5000x of magnification, acquired by scanning electron microscopy (SEM), using Inspect S50 instrument, FEI company. Three samples from each filter media were analyzed, with 5 images obtained for each sample (totaling 15 images per filter media). These images were used to determine the fiber diameter, the fiber diameter distribution, the superficial porosity, the density of intersections, and the maximum and minimum pore sizes. These determinations were performed with the DiameterJ plug-in of the ImageJ software package (Hotaling, 2015; Hotaling *et al.*, 2015). The characteristic pore size was considered to be the arithmetic median between the maximum and minimum pore sizes, and the density of intersections was the number of fiber overlaps per area (density of intersections 100x100 px is the number of fiber overlaps x 10000 / total pixels in the image).

2.2.4. **Filtration tests**

Figure 4 shows the experimental unit used to determine the particle collection efficiencies in air filtration, permeabilities, and pressure drops of the plain substrates and the fiber-coated substrates. The apparatus consisted of an aerosol generator (Model 3079, TSI), a filtered air supply (Model 3074B, TSI), a diffusion dryer (Model 3062, TSI), a krypton-85 charge neutralizer (Model 3054,

TSI), a filter media apparatus, an americium-241 charge neutralizer, a flowmeter (Gilmont), and an SMPS (scanning mobility particle sizer) composed of an electrostatic classifier (Model 3080, TSI), a differential mobility analyzer, and a particle counter (Model 3776, TSI).

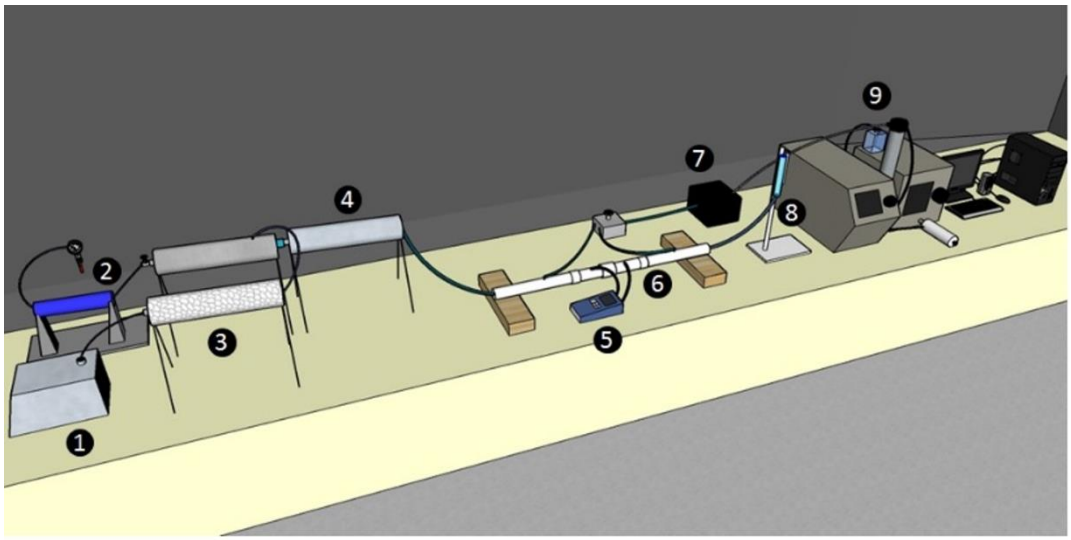

1 atomizer aerosol generator (TSI 3079), **2** filtered air supply (TSI 3074 B), **3** diffusion dryer (TSI 3062), **4** krypton 85 neutralizer (TSI 3054), **5** digital manometer (TSI 9555 P), **6** filter media apparatus, **7** americium 241 neutralizer, **8** flowmeter shielded tube size 12 (Gilmonte) and **9** scanning mobility particle sizer spectrometer – electrostatic classifier (TSI 3080) and ultrafine condensation particle counter (TSI 3776).

Figure 4. Schematic illustration of the system used for performance evaluation of the filter media.

Collection efficiency, permeability constant, and pressured drop were measured in all the experimental conditions shown in Table 1. The quality factor was calculated for M1 - M5.

2.2.4.1. Collection efficiency

The collection efficiency was evaluated for particles in the size range from 5 to 100 nm. The particles were generated by passing a solution of 0.1 g/L NaCl through the aerosol generator. The particle concentrations before and after the filter media were determined using the SMPS, one hour after the start of the test. The filtration area was 5.2 cm² and the face velocity was kept at 4.8 cm/s. The collection efficiency was calculated using Equation 19:

$$E = \frac{(C_0 - C_1) * 100}{C_0} \quad (19)$$

where E is the collection efficiency (%), C_0 is the particle concentration before the filter media (dW/dlogDp), and C_1 is the particle concentration after the filter media (dW/dlogDp).

2.2.4.2. Pressure drop

The pressure drop was measured using a digital manometer (VelociCalc Model 3A-181WP09, TSI) connected to the filtration apparatus as shown in Figure 4, as described by Barros et al (2016).

2.2.4.3. Permeability constant

Filter media permeability experiments were performed varying the face velocity from 0.3 to 6.4 cm/s, and the pressure drop was measured as described in the previous topic. Permeability constant (k) of each filter media was obtained using Darcy's law (Barros, Tanabe and Aguiar, 2016):

$$\frac{\Delta P}{L} = \frac{\mu v_L}{K} \tag{20}$$

where ΔP is the pressure drop (Pa), L is the thickness of the filter media (cm), μ is the air viscosity (1.74×10^{-7} Pa s), v_L is the face velocity (cm/s), and k is the permeability constant of the filter media (cm^2).

The thickness of the filter media was measured using an optical microscope (Model BX60, Olympus).

2.2.4.4. Quality factor

The quality factor relates pressure drop and collection efficiency and allows comparison between filter media, was calculated as follows:

$$Q_f = \frac{-\ln(1-E)}{\Delta P} \tag{21}$$

where Q_f is the quality factor (Pa^{-1}), E is the collection efficiency, and ΔP is the pressure drop (Pa).

2.2.5. **Statistical tests**

Tukey's test was used to evaluate the statistical significance between groups, considering the confidence level of 90% ($p < 0.1$).

2.3. RESULTS AND DISCUSSIONS

2.3.1. **Characterization of the substrates**

The filter media used as substrates for the spun fiber layers were evaluated in terms of their thickness, grammage, resin content, corrugation and performance in filtration assays, as shown in TABLE 2. The substrates were ordered from S1 to S5, in increasing order of permeability constant. S1, S2, S3, and S4 were composed of cellulose, while S5 was composed of polyester. The ranges obtained were 414 - 870 µm (thickness), 119 – 132 g/m^2 (grammage), 3.7 - 85.0 Pa (pressure drop), 3.79 x 10^{-4} - 187.13 x 10^{-4} cm^2 (permeability constant), and 41.8 - 58.7% (collection efficiency).

Table 2. Thicknesses and results of filtration test for substrates S1 - S5.

	S1	S2	S3	S4	S5
Thickness (µm)	414	375	495	619	870
Grammage (g/m^2)	121	122	119	119	132
Resin content (%)	15	-	15	14	-
Corrugation	No	Yes	No	No	No
Pressure drop (Pa)	85.0 ± 0.6	44.8 ± 0.5	41.1 ± 1.0	9.8 ± 0.5	3.7 ± 0.2
Permeability constant (cm^2) x 10^{-4}	3.79 ± 0.04	6.51 ± 0.01	9.57 ± 0.23	48.77 ± 1.61	187.13 ± 7.78
Collection efficiency (%)	58.7 ± 2.7	53.3 ± 2.8	56.0 ± 3.4	41.8 ± 3.0	42.5 ± 4.3

2.3.2. **Evaluation of fiber layer and filtration performance**

2.3.2.1. Effect of substrate

The fiber layers were spun, under the same operating conditions, onto the surfaces of all the substrates (S1-S5). At the end of the processes, the layers were characterized in terms of superficial porosity, pore size, fiber diameter, and density of intersections (Table 3). The fiber diameter varied from 0.84 to 0.93 µm, pore size from 5.6 to 9.2 µm, the density of intersections from 0.01 to 0.03 int/µm^2, and superficial porosity from 77 to 87%. These variations indicated that the fiber layers presented different characteristics, despite being produced under the same operational conditions, suggesting that the type of substrate affected the fibers produced. This fact was attributed to the use of VCS associated with different substrate permeability constant. The substrate

with higher permeability constant has lower internal resistance to airflow, allowing the suction provided by VCS to be higher, resulting in larger amounts of fibers deposited on the substrate surface, thus the porosity of the substrate decreases. Images of the fibers deposited on the different filter media are shown in Figure 5 (a- j).

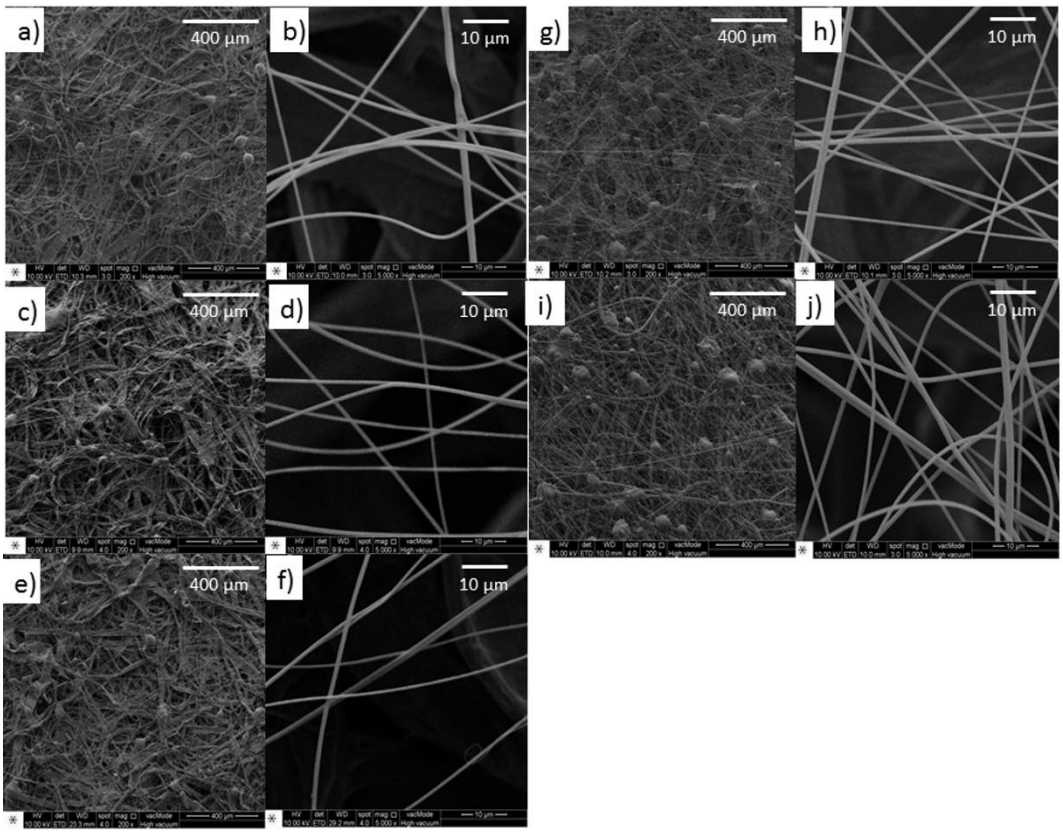

Figure 5. SEM images of the fiber layers at 200x and 5000x magnification for filters M1 (a, b), M2 (c, d), M3 (e, f), M4 (g, h), and M5 (i, j).

To evaluate the VCS effect, the density of fiber intersections and the superficial porosity of the fiber layer were investigated relative to the substrate permeability constant (Figure 6). It was found that the superficial porosity of the fiber layer decreased as the substrate permeability constant increased. Consequently, the density of fiber intersections showed the opposite behavior, increasing as the substrate permeability constant increased. The filter M5 has a polyester substrate while others are cellulose. Certainly, substrates of different materials affect the formation of the fiber layer as can be seen in the study by Nicosia *et al.* (2016), who observed that the arrangement of the fiber layer is influenced by the morphology of the substrate. However, the permeability

constant of the substrate was shown to change the characteristics of the spun fiber layer more significantly than the composition of the substrate.

Table 3. Characterization of the fiber layer: fiber diameter, pore size, density of intersections, and superficial porosity.

	M1	M2	M3	M4	M5
Fiber diameter (µm)	0.93 ± 0.33[a]	0.93 ± 0.33[a]	0.84 ± 0.26[a]	0.90 ± 0.28[a]	0.93 ± 0.32[a]
Pore size (µm)	8.7 ± 6.6[a]	9.2 ± 6.4[a]	7.4 ± 6.0[a]	6.5 ± 4.9[a]	5.6 ± 4.1[a]
Density of intersections (int/µm^2)	0.01	0.01	0.01	0.02	0.03
Superficial porosity (%)	87 ± 3[a]	86 ± 4[a]	87 ± 4[a]	82 ± 5[a]	77 ± 7[a]

The superscript lowercases represent the Tukey test for multiple comparisons between rows of each assay.

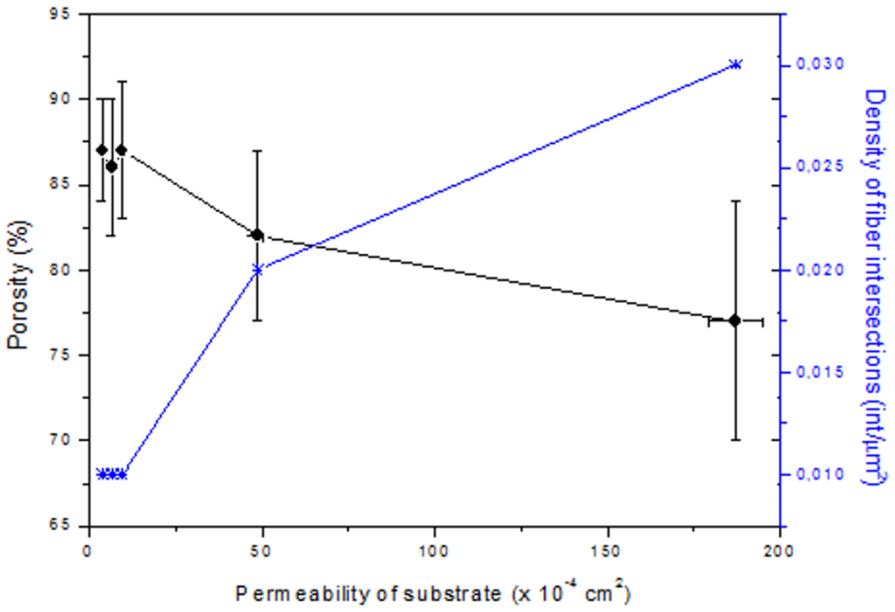

Figure 6. Substrate porosity and density of fiber intersections for the fiber layers spun over substrates with different permeability.

The fiber diameter distributions are shown in Figure 7 (a, b, c, d, e). Filters M1, M2, and M5 all presented a mean fiber diameter of 0.93 µm, while filters M3 and M4 presented mean fiber diameters of 0.84 and 0.90 µm, respectively. All the standard deviations were around 0.30 µm. Despite the different mean diameters, the diameter range with the highest frequency was 0.70 to 1.00 µm in all cases. The use of a VCS indicated that the VCS promoted fiber union. The images at 5000x magnification revealed the linking of the fibers on all the filters.

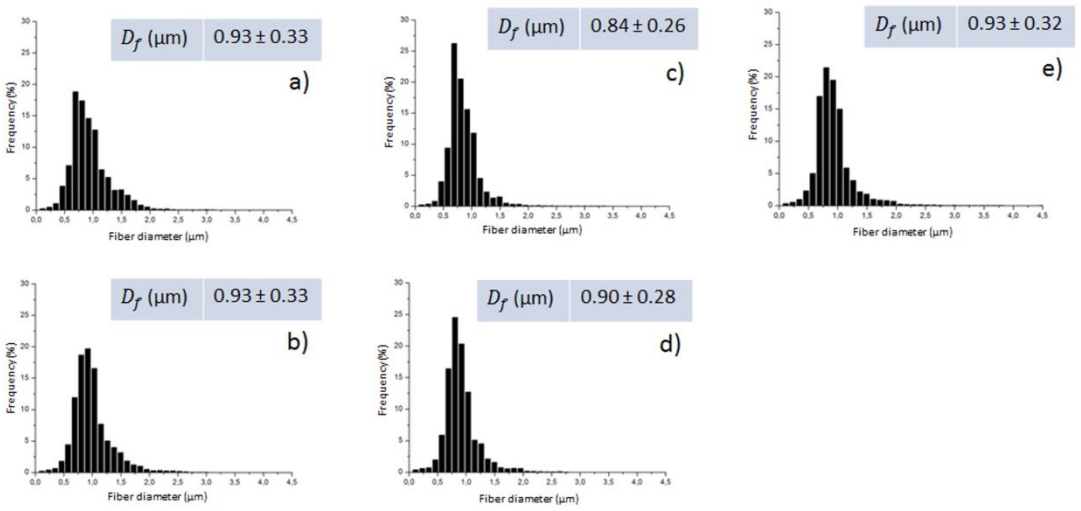

Figure 7. Fiber diameter distributions for filters M1 (a), M2 (b), M3 (c), M4 (d), and M5 (e).

2.3.2.2. Air filtration performance of the modified filter media

The performance of the fiber-covered filter media in air filtration was obtained for all fiber-covered substrates (Table 4). The results showed that the particle collection efficiency and pressure drop increased with the addition of the fiber layer to the substrates. This increase was due to the reduction in permeability constant, which increases the airflow resistance between the fibers, increasing the pressure drop and the collection efficiency of the filter media. Filter M5 presented the best quality factor, with a value of 0.11. Filter M1 showed the highest collection efficiency, while the highest variation of collection efficiency was obtained for filter M4. Although the characteristics of the fiber layer not statistically significant (Table 3), these small changes led to changes in collection efficiency, as there were different values of collection efficiency variation (Table 4). These features could be explained by the interactions of the effects due to the fiber diameter, pore size, and superficial porosity of the fiber layer (Table 3).

Table 4. Results of filtration tests using the fiber-covered substrates M1-M5.

	M1	M2	M3	M4	M5
Pressure drop (Pa)	88.7 ± 1.3[a]	47.0 ± 0.7[b]	42.7 ± 1.9[c]	12.5 ± 0.6[d]	6.0 ± 0.1[e]
Permeability constant (cm^2) x 10^{-4}	3.77 ± 0.11[a]	6.48 ± 0.37[b]	9.29 ± 0.22[c]	43.08 ± 0.34[d]	125.23 ± 0.09[e]
Collection efficiency (%)	63.2 ± 1.5[a]	54.8 ± 2.8[b]	62.5 ± 1.7[a]	51.8 ± 2.2[a,c]	48.1 ± 3.0[c]
Quality factor (Pa^{-1})	0.01	0.02	0.02	0.06	0.11
Collection efficiency variation (%)	4.5	1.5	6.5	10	5.6

The superscript lowercases represent the Tukey test for multiple comparisons between rows of each assay.

Figure 8 (a-e) shows the variation of the collection efficiency for particles in the size range from 5 to 100 nm, using the filter media without (S) and with (M) fiber coatings. Figure 8 (f) shows the particle size distribution. It can be seen from Figure 8 (a-e) that the collection efficiency decreased as the particle diameter increased. This behavior can be explained by the different contributions of the collection mechanisms, which are classified according to particle size to be collected; the collection mechanisms are interception, inertial impaction, diffusion, gravitational sedimentation, and electrostatic attraction (Hinds, 1999; L V *et al.*, 2018). Particles above 400 nm diameter are captured due to impaction and interception mechanisms. Particles with a diameter between 100 and 400 nm, which are considered the most penetrating and least effective for fibrous filters, are generally captured by the diffusion and interception mechanisms. However, particles in this range are too large to be collected by diffusion and too small to be collected by inertial impaction and interception. Therefore, the efficiency of the filter media decreases within this range (TSI, 2012). The diffusion mechanism becomes dominant for particles smaller than 100 nm that promoted increasing in the collection efficiency values.

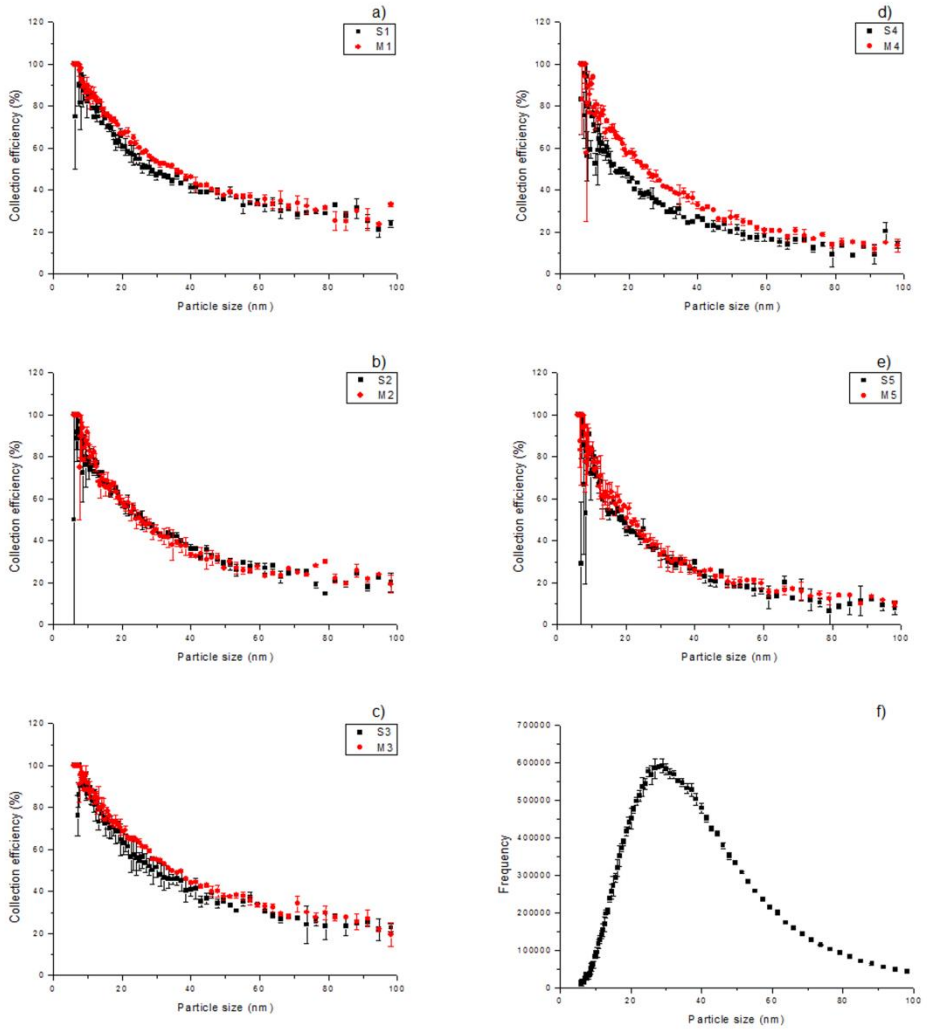

Figure 8. Collection efficiencies, according to particle size, for the different filter media: a) S1 and M1, b) S2 and M2, c) S3 and M3, d) S4 and M4, e) S5 and M5; f) particle size distribution.

To evaluate the effect of operating parameters on fiber production to air filtration, the following parameters were evaluated: VCS power, rotation speed, needle diameter, and collection time. The substrate S4 was selected to make this evaluation. The choice of this substrate was due to the greater variation in collection efficiency (10%) observed for the M4 filter medium (Figure 8).

2.3.2.3. Effect of VCS power

In order to evaluate the influence of the VCS power setting on the characteristics of the fiber layer and in the air filtration performance, fibers were spun on substrate S4 using 12 wt.% PAN solution and VCS powers ranging from 25 to 100%, the other parameters were kept the same as M4. Figure 9 shows SEM images of the fiber layers obtained using the different VCS power

settings. Table 5 shows the resulting collection efficiencies, pressure drops, fiber diameters, permeability constant, and superficial porosities of the fiber layers. The collection efficiency and pressure drop increased with the increase of the VCS power, while the superficial porosity and permeability constant decreased. These observations were in agreement with the paper of Wang et al. (2008), who reported that a decrease in the porosity of the fiber layer caused increases in both pressure drop and collection efficiency (Wang, Kim and Pui, 2008).

It was found that the fiber diameter decreased and collection efficiency increased as the VCS power was increased. Balgis et al (2015) and Yun et al (2010) shown that a smaller average fiber diameter can significantly improve the collection efficiency. However, it is important to highlight that there was also a decrease in superficial porosity, which could positively influence the collection efficiency (Wang, Kim and Pui, 2008). Although surface porosity is not statistically significant, the amount of fibers is visually noticeable as can be seen in Figure 8. The use of the VCS probably altered the trajectory of the jet formed around the spinneret, hence changing the characteristics of the fiber layer (Table 5). The increase in the VCS power could have caused the elongation of the fibers leading to fiber diameter decrease.

Table 5. Effects of VCS power on collection efficiency, pressure drop, permeability constant, fiber diameter, and superficial porosity.

Filter media	Collection efficiency (%)	Presure drop (Pa)	Permeability constant (cm^2) x 10^{-4}	Fiber diameter (µm)	Superficial porosity (%)
S4	41.8 ± 3.0^{a}	9.8 ± 0.5^{a}	48.77 ± 1.61^{a}	-	-
VCS25	48.4 ± 0.2^{b}	10.0 ± 0.1^{a}	$46.72 \pm 1.62^{a,b}$	1.24 ± 0.34^{a}	93 ± 3^{a}
VCS50	50.0 ± 1.5^{b}	11.4 ± 0.2^{b}	44.39 ± 1.38^{b}	1.26 ± 0.50^{a}	87 ± 4^{a}
VCS75	50.2 ± 2.3^{b}	11.7 ± 0.1^{b}	43.48 ± 0.12^{b}	1.15 ± 0.41^{a}	78 ± 7^{a}
M4	51.8 ± 2.2^{b}	12.5 ± 0.6^{b}	43.08 ± 0.34^{b}	0.90 ± 0.28^{a}	82 ± 5^{a}

The superscript lowercases represent the Tukey test for multiple comparisons between columns of each assay.

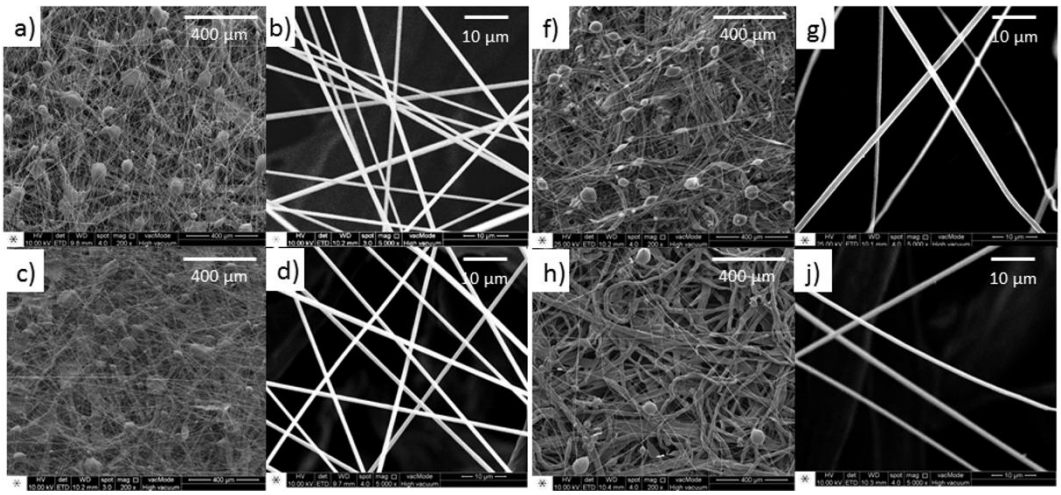

Figure 9. SEM images of the fiber layers at 200x and 5000x magnification obtained using different VCS power settings: 100% (a, b), 75% (c, d), 50% (e, f), and 25% (g, h).

2.3.2.4. Effect of collection time

Fibers were spun on substrate S4 using collection times of 60 and 180 s, the other parameters were kept the same as M4. The resulting media were denoted M4 and T180, respectively. Table 6 provides the values obtained for the collection efficiency, pressure drop, superficial porosity, permeability constant, and fiber diameter. The collection efficiencies were similar for M4 and T180, with values of around 52%. However, there was a substantial difference in the fiber diameters, with values of 0.90 µm for M4 and 2.51 µm for T180, which provided further evidence of fiber union induced by the reverse airflow promoted by VCS.

The pressure drop was higher for M4 (12.5 Pa) than for T180 (11.4 Pa), which could be explained because the thinner fibers provided higher resistance to the passage of air. The pressure drop increases significantly when the fiber diameter decreases, even in the slip regime (Brown, 1993). Figure 10 shows SEM images of the fiber layers obtained using collection times of 60 and 180 s. M4 has a superficial porosity of 82% while T180 has 76%. Agubra *et al*. (2016) employed the Forcespinning technique with 12% PAN solution, using similar operational parameters (30G½" needles, 8000 rpm rotation speed, and a VCS), and obtained an average fiber diameter smaller than 4 µm (Agubra *et al.*, 2016). It was observed that the fiber diameter was influenced by the collection time.

Table 6. Effect of fiber collection time on filter media collection efficiency, pressure drop, superficial porosity, and fiber diameter.

Filter media	Collection efficiency (%)	Pressure drop (Pa)	Permeability constant (cm^2) x 10^{-4}	Fiber diameter (μm)	Superficial porosity (%)
S4	41.8 ± 3.0[a]	9.8 ± 0.5[a]	48.77 ± 1.61[a]	-	-
M4	51.8 ± 2.2[b]	12.5 ± 0.6[b]	43.08 ± 0.34[b]	0.90 ± 0.28[a]	82 ± 5[a]
T180	52.1 ± 0.2[b]	11.4 ± 0.4[a]	44.18 ± 0.01[b]	2.51 ± 1.22[b]	76 ± 9[a]

The superscript lowercases represent the Tukey test for multiple comparisons between columns of each assay.

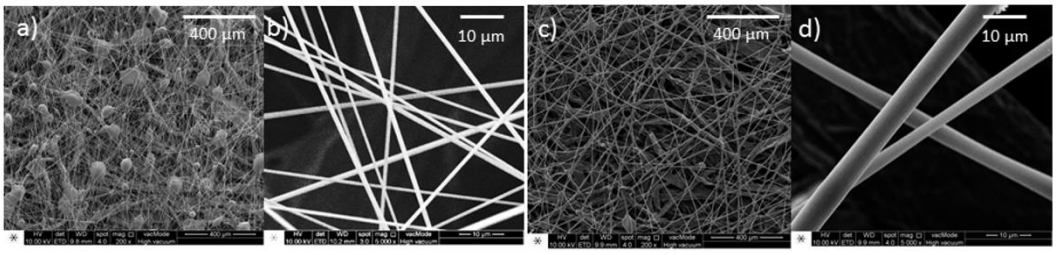

Figure 10. SEM images of the fiber layer at 200x and 5000x magnification obtained using collection times of 60 (a, b) and 180 s (c, d).

2.3.2.5. Effect of rotation speed

The rotation speed is an important parameter because the centrifugal force, together with the influence of the air frictional force, causes elongation of the liquid jets, hence leading to the formation of fibers (Zhang and Lu, 2014). The effect of rotation speed was evaluated by spinning the fibers on substrate S4 at velocities of 4000 and 6000 rpm (denoted M4 and V6000, respectively), the other parameters were the same as M4. Table 7 shows the values obtained for the collection efficiency, pressure drop, fiber diameter, permeability constant and superficial porosity of the filter media. The fiber diameter was around 0.90 μm for both, while the collection efficiency was lower for V6000 (46.7%) than for M4 (51.8%). Even though the surface porosity, fiber diameter, and permeability constant were statistically non-significant, these small differences should have caused the increase in the collection efficiency of M4, due to the lower superficial porosity, fiber diameter, and permeability constant of M4. That is, the V6000 has a higher permeability constant than M4, causing a reduction in pressure drop due to increased porosity and this must have reduced efficiency. This behavior may have occurred due to fiber agglomeration, leaving more voids in the fiber layer. Figure 11 shows SEM images of the fiber layers

obtained using the different rotation speeds. Lu *et al*. (2013) evaluated the influence of rotation speed on PAN fibers spun without the use of a VCS and found that the fiber diameter decreased as the rotation speed was increased (Lu *et al.*, 2013). The different behaviors observed by Lu *et al*. (2013) and in the present study evidenced that the use of the VCS collector influenced the fiber deposition and changed the characteristics of the fiber layer.

Table 7. Effect of rotation speed on collection efficiency, pressure drop, fiber diameter, and superficial porosity.

Filter media	Collection efficiency (%)	Pressure drop (Pa)	Permeability constant (cm^2) x 10^{-4}	Fiber diameter (μm)	Superficial porosity (%)
S4	41.8 ± 3.0[a]	9.8 ± 0.5[a]	48.77 ± 1.61[a]	-	-
M4	51.8 ± 2.2[b]	12.5 ± 0.6[b]	43.08 ± 0.34[b]	0.90 ± 0.28[a]	82 ± 5[a]
V6000	46.7 ± 4.3[c]	10.5 ± 0.7[a,b]	45.54 ± 2.27[a,b]	0.93 ± 0.32[a]	85 ± 6[a]

The superscript lowercases represent the Tukey test for multiple comparisons between columns of each assay.

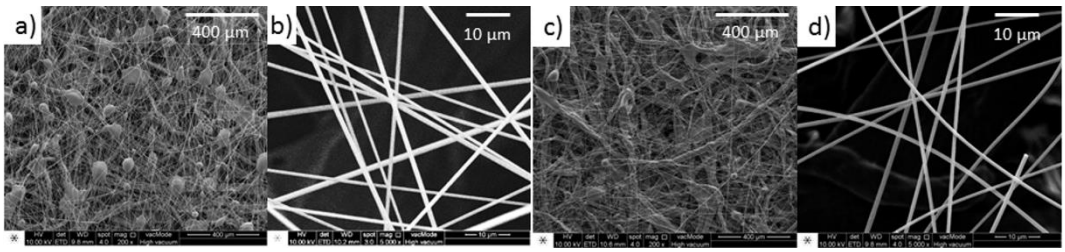

Figure 11. SEM images of the fiber layer at 200x and 5000x magnification obtained using rotation speeds of 4000 rpm (a, b) and 6000 rpm (c, d).

2.3.2.6. Effect of needle diameter

In order to evaluate the effect of needle diameter, the fibers were spun on substrate S4 using two different needle sizes (26G½" and 30G½", denoted M4 and N30, respectively) with other parameters same as M4. Table 8 shows the values obtained for the collection efficiency, pressure drop, permeability constant, superficial porosity, and fiber diameter. M4 has a surface porosity of 82% while N30 has 89%. SEM images of the fiber layers obtained using the different needles are shown in Figure 12. Lu *et al*. (2013) evaluated the influence of needle diameter on PAN fibers spun without the use of a VCS and concluded that the fiber diameter decreased as the needle diameter decreased (Lu *et al.*, 2013). However, in the present work, the fiber diameter was lower for M4 (0.90 μm), compared to N30 (1.16 μm). This behavior may have occurred

due to fiber agglomeration in the N30 fiber layer, leaving more voids in the fiber layer. The pressure drop was 12.5 Pa for M4 and 10.4 Pa for N30, which could be explained because of the thinner fibers because the pressure drop increases significantly when the fiber diameter decreases (Brown, 1993). M4 has a smaller permeability constant than N30, causing an increase in pressure drop due to decreased porosity and this must have increased collection efficiency. Higher collection efficiency (51.8%) was obtained for M4, compared to N30 (45.5%), which could be explained by the lower superficial porosity, fiber diameter, and permeability constant for M4. Because that even permeability constant, fiber diameter and superficial porosity were statistically non-significant, these small differences should have caused the increase in the collection efficiency. This provided another indication of the effect of the VCS on the fibers produced.

Table 8. Effect of needle diameter on collection efficiency, pressure drop, superficial porosity, and fiber diameter.

Filter media	Collection efficiency (%)	Pressure drop (Pa)	Permeability constant (cm^2) x 10^{-4}	Fiber diameter (µm)	Superficial porosity (%)
S4	41.8 ± 3.0^{a}	9.8 ± 0.5^{a}	48.77 ± 1.61^{a}	-	-
M4	51.8 ± 2.2^{b}	12.5 ± 0.6^{b}	43.08 ± 0.34^{b}	0.90 ± 0.28^{a}	82 ± 5^{a}
N30	45.5 ± 5.4^{a}	10.4 ± 0.1^{a}	$45.93 \pm 1.54^{a,b}$	1.16 ± 0.42^{a}	89 ± 3^{a}

The superscript lowercases represent the Tukey test for multiple comparisons between columns of each assay.

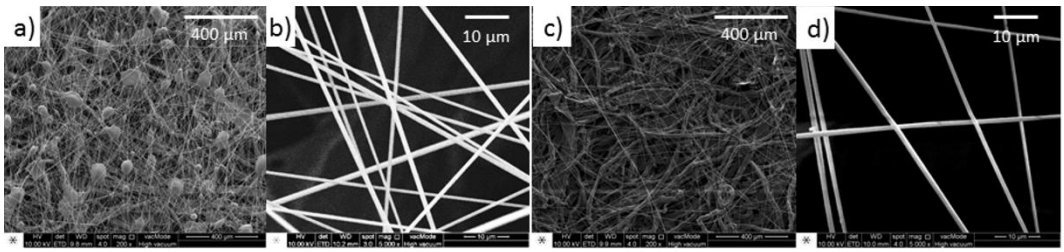

Figure 12. SEM images of the fiber layer at 200x and 5000x magnification obtained using needles with diameters of 26G (a, b) and 30G (c, d).

2.4. CONCLUSIONS

This paper studied the influence of the vacuum collection system (VCS) on fibers produced by the Forcespinning technique. The effects of filter media type used as the substrate, besides VCS power, collection time, rotation speed, and needle diameter were evaluated on the fiber layer characteristics and the

filtration performance of ultrafine particles. In the evaluation of the different types of substrates as the main result, it was found that the combination of the use of a VCS and substrates with different permeability constant led to the formation of fiber layers with different characteristics in terms of fiber diameter, porosity, and pore size. The higher the permeability constant of the substrate was higher density of fiber intersections in the layer of spun fiber. The VCS power analysis showed that increasing the VCS power promoted the increase in collection efficiency and pressure drop and the decrease in superficial porosity and fiber diameter. The evaluation of collection times, 60 (M4) and 180 s (T180) resulted in similar collection efficiencies, although the pressure drop was higher for M4 than for T180. The data showed that increasing the collection time promoted an increase in the fiber diameter. In tests to evaluate the effects of rotation speed and needle diameter, it was observed that even very small differences between the variables affected the collection efficiency of the nanoparticle. This research is encouraging and indicates that the VCS can be used to improve the performance of the filter media. However, further studies are needed in order to increase the collection efficiency. Further improvements can be achieved by evaluating a greater range of operational settings, especially the VCS power and the collection time. In addition, the systematic study of VCS collector utilization will contribute to researchers from all research areas that use this technique.

3. FILTRATION PERFORMANCE OF PAN FIBER PRODUCED BY CENTRIFUGAL SINNING USING DMSO AND DMF AS SOLVENT

3.1. INTRODUCTION

Polyacrylonitrile (PAN) has been used as fiber for good stability and mechanical properties. Liu et al. (2015) reported that fibers with higher dipole moments, as PAN fibers, had higher particulate matter (PM) capture efficiency. PM is a functional group of high polarities distributed on the surface and PAN has a higher dipole moment that can have stronger dipole-dipole and induced-dipole inter-molecular forces, which improves particle capture (Liu *et al.*, 2015). PAN is soluble in polar solvents as dimethylformamide (DMF), dimethyl sulfoxide (DMSO), dimethylacetamide, dimethyl sulfone, tetramethylsulfide. PAN solubility parameter is 25.3, DMF is 24.8 and DMSO 26.6 $MPa^{1/2}$. DMF and DMSO are solubility parameters comparable to PAN, for that they are good solvents. Even though DMF dissolves PAN faster than DMSO, DMSO provides less health and environmental risks than DMF (“Safety Data Sheet - DMF”; “Safety Data Sheet - DMSO”). Besides DMSO promoted high orientation and crystallinity to PAN and solved with higher stability and wider processing window (Eom and Kim, 2014; Zeng *et al.*, 2007).

There are many methods for produce thinner fibers: melt blown (Medeiros *et al.*, 2009), solution blowing spinning (Mahalingam and Edirisinghe, 2013), pressurized gyration process (Deitzel *et al.*, 2001) and electrospinning (Padron *et al.*, 2013). Centrifugal spinning has been a promising method of produce polymeric fibers, in micro and nanoscale, using centrifugal forces. This process has been researched for being highly productive and reducing production costs (Padron *et al.*, 2013; Sarkar *et al.*, 2010).

Therefore, this study aimed to evaluate fiber diameter, pore area, superficial porosity and filtration performance of filter media covered with fibers produced by Forcespinning (centrifugal spinning method) from PAN dissolved in DMF and DMSO.

3.2. MATERIALS AND METHODS

3.2.1. **Materials**

Commercial filter media was used as substrate. Polyacrylonitrile (PAN, Mw: 150,000 g/mol) and N, N-dimethylformamide (DMF, anhydrous, 99.8%) were purchased from Sigma-Aldrich® and dimethyl sulfoxide (DMSO, anhydrous, 99.9%) was purchased from Synth**.**

3.2.2. **Preparation of the fibers**

PAN (12 wt. %) was dissolved in DMF and DMSO by heating (60 °C) and stirring for 4 hours to prepare the fibers. The fiber layer was covered over the substrate using the technique of centrifugal spinning by Forcespinning™ (FS) and vacuum collecting system (VCS) as the collector. The FS operational conditions were 26-gauge half-inch needle, 10 cm needle-collector distance, rotational speed was 4000 rpm, 60 s collection time, VCS on 100% power and room pressure and temperature.

3.2.3. **Characterization and filtration performance**

These fiber diameter, fiber diameter distribution, superficial porosity, pore area were performed using plugin DiameterJ on ImageJ software from SEM images (FEI Company, Inspect S50). The collection efficiency is commonly calculated by Equation 22:

$$E = \frac{(C_0 - C_1) * 100}{C_0} \tag{22}$$

where E is collection efficiency, C_0 is the particle concentration before filter media and C_1 is the particle concentration after filter media.

The nanoparticles were generated from a solution of 0.1 g/l NaCl through the atomizer aerosol generator (TSI 3079). The concentration of the particles before and after the filter media was determined by the scanning mobility particle sizer spectrometer (TSI 3080), one hour after the start of the test. The filtration rate was maintained at 4.8 cm/s and the filtration area was 5.2 cm². The particle size ranged from 6 to 100 nm.

The pressure drop was measured by the digital manometer (TSI 9555 P) at the beginning of the experiment.

3.3. RESULTS AND DISCUSSIONS

PAN (12 wt. %) solutions dissolved in DMF and DMSO were spun on the substrate over the same operational conditions. The filters were named DMSO and DMF according to the solvent. SEM image of fiber layer spun over DMF, Figure 13 (a) and (c), and DMSO, Figure 13 (b) and (d), were performed on Inspect S50, FEI Company.

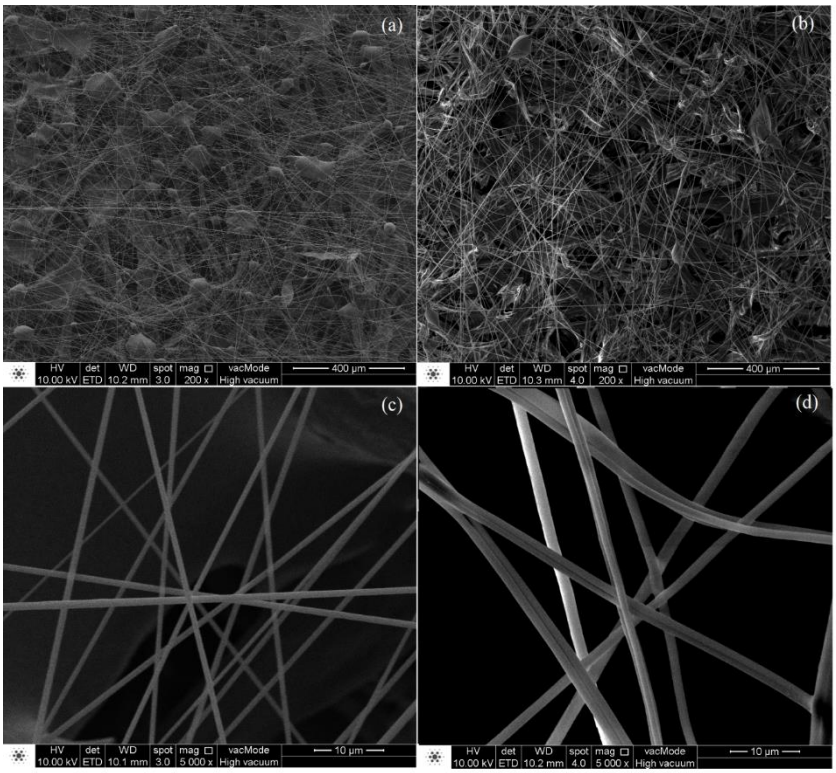

Figure 13. SEM image of fiber layer: (a) DFM and (b) DMSO at 200x magnification and (c) DMF and (d) DMSO at 5000x magnification.

DMF and DMSO fiber layers were characterized according to fiber diameter, pore area, and superficial porosity, Table 8. DMF was fiber diameter smaller than DMSO, 0.90 and 1.56 μm respectively. The superficial porosity was close value around 82% and the pore area were 49.2 and 85.0 μm^2, respectively to DMF and DMSO. Although superficial porosities were close values, fiber diameter and pore area were a large difference.

Figure 14 shows the fiber diameter of DMF and DMSO in percentual. DMF has a high level of fiber ranging from 0.25 to 0.5 um and DMSO has ranging 0.50 to 0.75 μm.

Table 8. Fiber layer characterization: fiber diameter, pore area and superficial porosity.

	DMF	DMSO
Fiber diameter (µm)	0.90 ± 0.28	1.56 ± 0.68
Pore area (µm^2)	49.2 ± 22.3	85.0 ± 72.1
Superficial porosity (%)	82 ± 5	83 ± 5

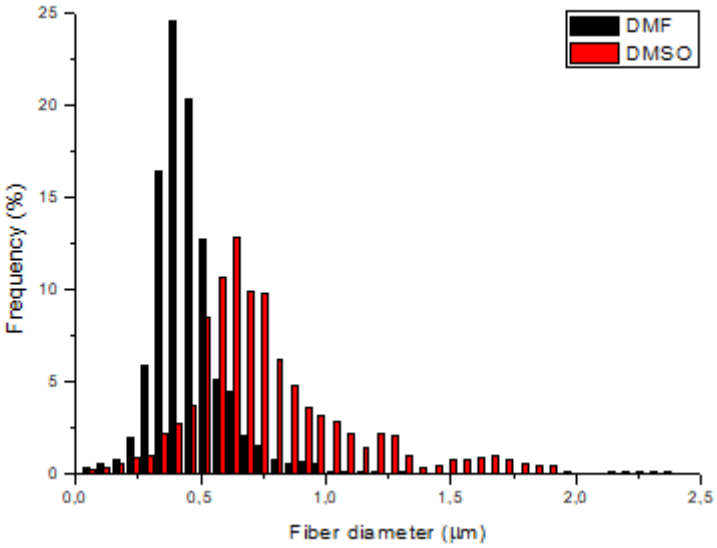

Figure 14. Frequency in percent of DMF and DMSO fiber diameter.

Balgis *et al.* (2015) and Yun *et al.* (2010) noticed that efficiency improves significantly with the reduction of the average diameter. How DMF was thinner fiber than DMSO, it is expected that DMF was higher collection efficiency than DMSO, but both were close collection efficiency as can be seen in Figure 14. Liu *et al*. (2015) reported that PM has functional groups of high polarities distributed on surface and fiber that have higher dipole moment (promotes stronger dipole-dipole and induced-dipole inter-molecular forces) improves particle capture. Eom and Kim (2014) detected that the solvent DMF takes resonance structure and DMSO takes fixed charged distribution on PAN solution. These indicate that the solvent DMSO promotes stronger and more consistent polarization than DMF, which would lead to higher collection efficiency. This can explain DMSO and DMF filter media were collection efficiency close, even, DMF was fiber diameter and pore size smaller than DMSO. DMF was pressure drop, 12.5 Pa, higher than DMSO, 10.4 Pa. However, DMF collection efficiency was 51.8% and DMSO 55.2%.

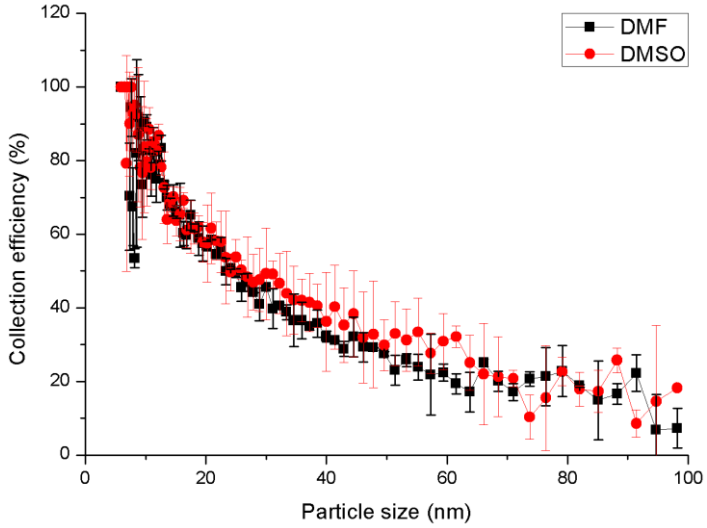

Figure 15. DMF and DMSO collection efficiency for particle size that ranged from 5 to 100 nm.

3.4. CONCLUSION

This work compared fiber diameter, pore area, superficial porosity and filtration performance of substrate covered with PAN fibers spun from DMF and DMSO solutions.

DMSO had pore area and fiber diameter higher than DMF. The superficial porosity of the filter media had a very close value. DMF had a pressure drop of 12.5 Pa and a collection efficiency of 51.8% while DMSO was 10.4 Pa and 55.2%, respectively. Even DMF having fiber diameter and pore size smaller than DMSO, the collection efficiency was close value. This can indicate that the DMSO promotes stronger and more consistent polarization in PAN than DMF, increasing the collection efficiency of the DMSO filter medium.

4. CHARACTERIZATION AND MICRO AND NANOPARTICLES FILTRATION EVALUATION OF PAN NANOFIBERS PRODUCED BY CENTRIFUGAL SPINNING

4.1. INTRODUCTION

Air pollution poses a significant environmental risk to human health. Particles when inhaled increases the risk of respiratory and cardiovascular diseases, diabetes, lung cancer, which can lead to premature death (Hayes *et al.*, 2019; Krauskopf *et al.*, 2019). Recent studies linked air pollution with Alzheimer's disease (Walton, 2018), dementia (Lee *et al.*, 2019), cerebral ischemic attack, epilepsy, and headaches (Radmanesh *et al.*, 2019).

Filter media is commonly used to control and remove particles from the air. The spun fiber has been researched for filtration application with excellent performance (Feng *et al.*, 2019; Zhu *et al.*, 2016). Spun fiber has a high surface-volume ratio, small pore size, and small fiber diameter that promote the increase of the collection efficiency of micro and nanoparticles. Fundamental parameters for filtration are collection efficiency and pressure drop. Collection efficiency is the number of particles captured by the filter media from the gas stream and pressure drop measures the resistance of air passage. A good filter media should have the maximum collection efficiency with the lowest pressure drop (Hinds, 1999).

Centrifugal spinning has been a promising method of produces polymeric fibers. Centrifugal spinning increases the choice of the materials, productivity, and reduces production cost (Padron *et al.*, 2013; Sarkar *et al.*, 2010). In recent papers, these fibers were used for battery (Flores *et al.*, 2018; Kim, 2019), tissue engineering (Lukášová *et al.*, 2019; Mamidi, Romo, Gutiérrez, *et al.*, 2019), adsorption (Kummer *et al.*, 2018; Rostamian, Firouzzare and Irandoust, 2019), colorimetric sensor for food (Valdez *et al.*, 2019), fibrous color dosimeter (Kinashi *et al.*, 2018), pharmaceutical application (Akia *et al.*, 2019; Mamidi, Romo, Barrera, *et al.*, 2019).

Given the above background, this work aims to evaluate the filtration performance of the substrate (without cover), and PAN nanofibers covered at the same substrate produced by Forcespinning (centrifugal spinning

equipment). For this, the characteristics of the fiber layer and collection efficiency of micro and nanoparticles were investigated.

4.2. MATERIALS AND METHODS

4.2.1. **Fiber preparation**

Forcespinning (FS) employs the centrifugal spinning to produce the nanofibers. This equipment consists of a spinneret, needles, metal bar, and vacuum collection system, which can be seen in Figure 16. The substrate (filter medium with a weight of 75 g/m^2) was fixed on the vacuum collection system at 5 cm from the lateral edges and 7.5 cm from the bottom edge. For fiber formation, the solution of 12 wt. % polyacrylonitrile (PAN, Mw: 150,000 g/mol, Sigma Aldrich) was dissolved in N,N-dimethylformamide (DMF, anhydrous, 99.8%, Sigma Aldrich), by heating (60 °C) and stirring at 3 hours. In the FS, the nanofiber was produced using 26-gauge half-inch needles, 10 cm needle-collector distance, 4000 rpm of rotation speed, 60 s of collection time, and 100% VCS power.

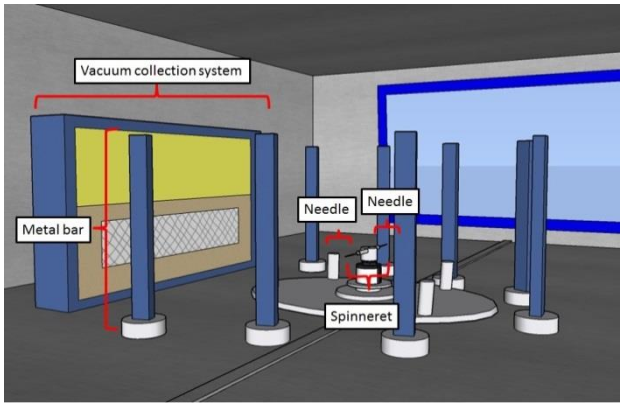

Figure 16. Schematic illustration of the arrangement of the Forcespinning system.

4.2.2. **Characterization of the fiber layer**

The nanofiber layer was characterized by scanning electron microscopy (SEM) using FEI Inspect S50. SEM images were used to determine the fiber diameter, the superficial porosity, the density of intersections, and pore size. The parameters were performed on the DiameterJ plug-in of the ImageJ software package.

4.2.3. **Filtration test**

The experimental unit used to perform the nanoparticle collection efficiency, permeability, and pressure drops of the substrate (without cover), and the substrate covered with PAN fiber can be seen in Figure 17. The apparatus consisted of the aerosol generator (Model 3079, TSI), filtered air supply (Model 3074B, TSI), diffusion dryer (Model 3062, TSI), krypton-85 charge neutralizer (Model 3054, TSI), filter media apparatus, americium-241 charge neutralizer, flowmeter (Gilmont), and scanning mobility particle sizer (SMPS) composed of electrostatic classifier (Model 3080, TSI), differential mobility analyzer, and particle counter (Model 3776, TSI). The nanoparticles were generated by aerosol generator from 0.1 g/L sodium chloride (NaCl, 99.7%, J. T. Baker) solution. The particle concentrations before and after the filter media were determined using the SMPS, 30 minutes after the start of the test. The filtration area was 5.3 cm² and the superficial gas velocity of 4.8 cm/s.

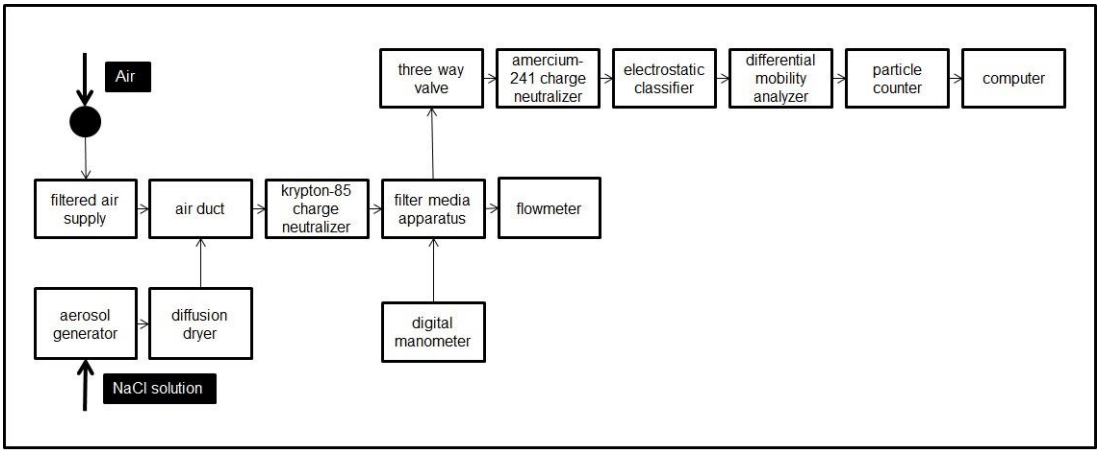

Figure 17. Flow chart of the system used to perform nanoparticle collection efficiency, permeability, and pressured drop of the filter media.

Figure 18 shows the experimental unit used to perform the microparticle collection efficiency. The experimental unit was composed of particle feeder (model 3433, TSI), diluter (model 3302A, TSI), aerodynamic particle sizer spectrometer (APS, model 3320, TSI), flowmeter (Gilmont), and pump. The microparticles were hydrated lime powder, the particle density is 2.7742 g/cm^3. The particle concentrations before and after the filter media were determined in APS, at the beginning and after 30 minutes of the start of the test. The filtration area was 17.6 cm² and the superficial gas velocity of 4.8 cm/s.

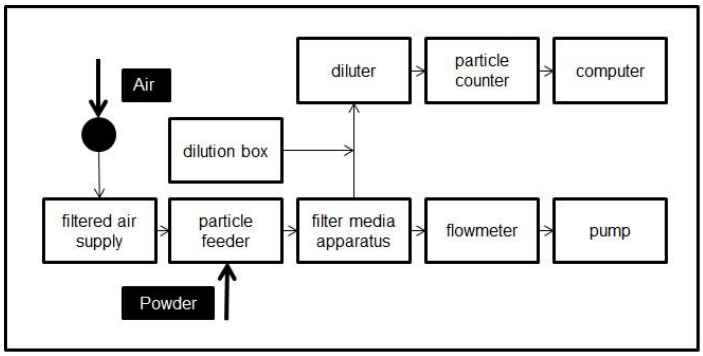

Figure 18. Flow chart of the system used to perform microparticle collection efficiency of the filter media.

The collection efficiency was determined using Equation 23:

$$E = \frac{(C_0 - C_1) * 100}{C_0} \quad (23)$$

where E is the collection efficiency, C_0 is the particle concentration before, and C_1 is the particle concentration after the filter media.

The pressure drop was measured using a digital manometer (Model 9555P, TSI) with a superficial gas velocity of 4.8 cm/s.

The permeability of each filter media was obtained from the equation for the linear plot of superficial gas velocity (ranged from 0.3 to 6.4 cm/s) against $\Delta P/L$, calculated using Darcy's law on Equation 24:

$$\frac{\Delta P}{L} = \frac{\mu v_L}{K} \quad (24)$$

where ΔP is the pressure drop, L is the thickness of the filter media, μ is the fluid viscosity, v_L is the superficial gas velocity, and k is the permeability constant of the filter media.

4.3. RESULTS AND DISCUSSION

4.3.1. **Characterization of the fiber layer**

SEM images were used on ImageJ software to measure the fiber diameter, superficial porosity, density of intersections, and pore size. PAN nanofiber layer was 1040 ± 400 ηm of the mean fiber diameter, 86 ± 5% of superficial porosity, 0.01 ± 0.01 int/μm^2 of the density of intersection, 7.0 ± 2.5 μm of pore size. Figure 19 shows the SEM image of PAN nanofibers with a) 5000 x and b) 200 x of magnification, and c) fiber diameter distribution. The

most frequent diameter was between 700 and 1000 ηm. These data report a single fiber layer with large fiber diameter dispersion and pore size.

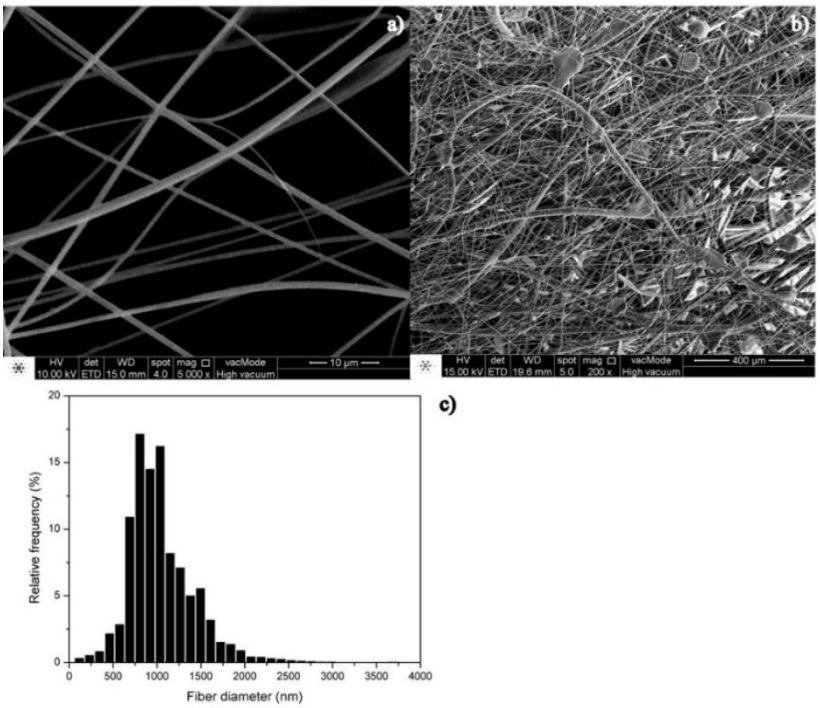

Figure 19. a) SEM image of PAN nanofiber layer with 5000 x and b) 200 x of magnification and c) fiber diameter distribution.

4.3.2. **Evaluation of filtration test**

The permeability shows the ease or difficulty of air passing through the filter medium. Figure 20 shows ΔP/L *versus* superficial gas velocity of the substrate and covered substrate. The determination coefficient (R^2) of the substrate and covered substrate were 0.989 and 0.999, respectively. It demonstrated that the curves are well adjusted. The substrate with PAN nanofibers presented a higher pressure drop than the substrate. Thus, the linear regression of the covered substrate had a high regression coefficient and the steepest curve. The substrate and covered substrate with PAN nanofiber permeability were 3.3 ± 0.0 10^{-5} m^2 and 1.5 ± 0.6 10^{-5} m^2, respectively. These values indicate that the substrate is more permeable than the covered substrate.

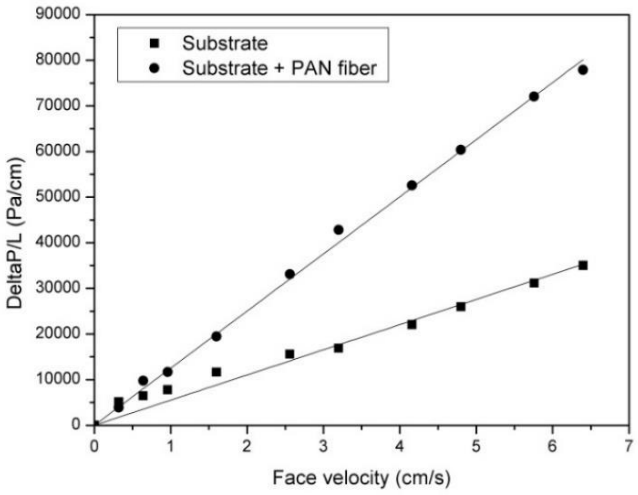

Figure 20. ΔP/L versus superficial gas velocity of substrate and substrate with PAN nanofibers.

Collection efficiency performed on the substrate and PAN nanofibers covered substrate for nano and microparticles, can be seen in Figures 21 a) and 22 a), respectively. For the collection efficiency of nanoparticles, the particles were generated from 0.1 g/l of NaCl solution by an aerosol generator in the experimental unit of Figure 17. The nanoparticle size ranged from 5.9 to 224.7 nm, and the largest concentration of particle was from 25 to 50 nm, as can be seen in Figure 21 b). The concentration of particles before and after filter media was measured 30 minutes after the beginning of the experiment. The substrate had a collection efficiency of 11.5%, while the substrate with a nanofiber layer had 31.3%, resulting in a difference of 19.8% (Table 9). This effect occurs because the addition of the fiber layer promotes increased particle capture. PAN nanofibers have a fiber mean diameter of 1040 nm, which fibers of this size are on the slip flow regime. On the slip flow regime, the gas fluid slip over the fiber surface, promoting greater interaction between the particles and the fiber, which increases the collection efficiency (Li *et al.*, 2014). Particles smaller than 100 nm have an increase in collection efficiency due to the predominance of diffusion collection mechanisms (Chuanfang, 2012). This behavior can be noticed in both curves, Figure 21 a). Similar results were obtained in the study by Bortolassi et al. (2019).

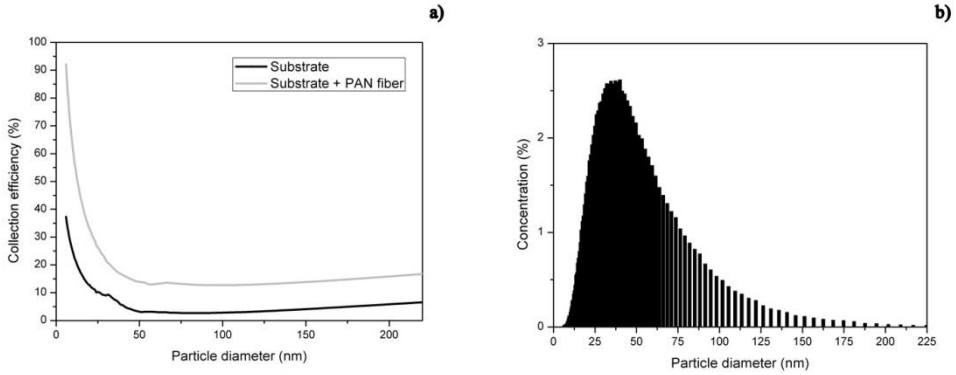

Figure 21. Collection efficiency performed on substrate and PAN nanofibers covered substrate for nanoparticles, and b) distribution of nanoparticles size.

The collection efficiency was also measured for hydrated lime microparticles, at the beginning (t=0) and after 30 minutes of the start of the test (t=30), as shown in Figure 22 a). The microparticles ranged from 1 to 19.8 µm, with the highest concentrations between 1 and 5 µm, as can be seen in Figure 22 b). The particle concentrations before and after the filter media were determined by APS in the experimental unit of Figure 18. At t=0, the substrate had a collection efficiency of 50.5%, and the covered substrate had 71.0%. The collection efficiency increased because of the addition of the fiber layer, just like in the previous case. But in this case, how the particles are large diameter, the predominant collection mechanisms are interception and inertial impaction, which promotes the increase of collection efficiency with the increase of particle size (Chuanfang, 2012). This behavior can be noticed in all curves, Figure 21 a).

After 30 minutes of filtration, the substrate remains in deep filtration, i.e., the powder has not accumulated sufficiently to form the cake. For the covered filter, the PAN fiber layer promoted surface filtration enabled the dust cake formation, which significantly increased particle collection. Thus, after 30 minutes of filtration, the substrate increased collection efficiency from 50.5 to 69.6%, while the covered substrate increased from 71.0 to 97.2% (Table 9). For example, for particle size 1.0 µm the collection efficiency of substrate + PAN fiber at t=0 was 36.7% and the substrate with PAN fiber at t=30 min was 92.9%, showing how the dust cake filtration influenced the collection efficiency.

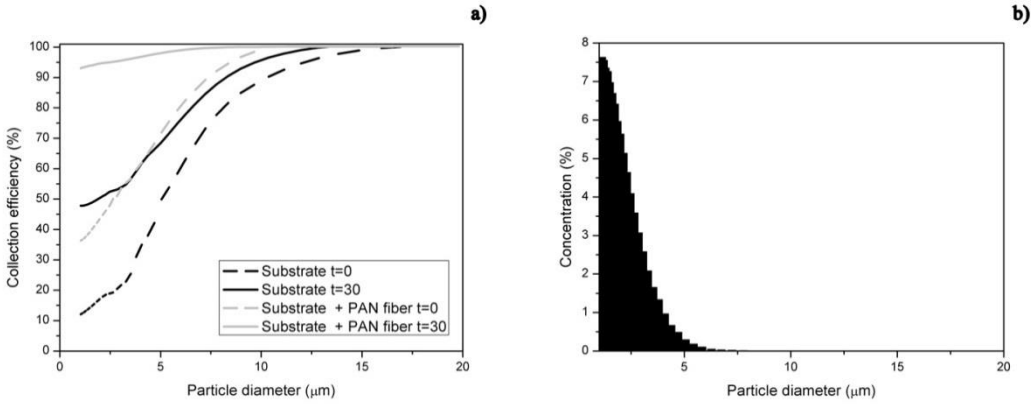

Figure 22. a) Collection efficiency performed on substrate and substrate covered with PAN nanofibers for microparticles at the beginning and 30 minutes after the start of the test, and b) distribution of microparticles size.

In terms of pressure drop, the substrate had an initial pressured drop of 0.6 Pa and the covered filter of 1.6 Pa. For nanoparticle filtration, there was no significant increase in pressure drop for both the substrate and the covered substrate. However, for microparticle filtration, the substrate increased from 0.6 to 1.2 Pa, and the covered substrate increased from 1.6 to 21.3 Pa, demonstrating that during the 30 minutes of filtration there was the formation of dust cake. Larger amount of particles was retained on the surface of the covered substrate, increasing the pressure drop value (Leung and Choy, 2018).

Table 9. Pressure drop and collection efficiency of micro and nanoparticles at the beginning and 30 minutes after the start of the test.

Filter media	Filtration time (min)	Collection efficiency (%)		Pressured drop (Pa)	
		nanoparticles	micro particles	nanoparticles	micro particles
Substrate	0	-	50.5 ± 12.7	0.6 ± 0.1	0.6 ± 0.1
Substrate + PAN fiber	0	-	71.0 ± 7.1	1.6 ± 0.6	1.6 ± 0.6
Substrate	30	11.5 ± 5.8	69.6 ± 6.7	0.6 ± 0.2	1.2 ± 0.1
Substrate + PAN fiber	30	31.3 ± 5.1	97.2 ± 2.2	2.6 ± 0.3	21.3 ± 1.0

The addition of the fiber layer promoted a significant increase in collection efficiency without a significant increase in pressure drop. Wang et al. (2008) studied filters composed of a layer of fibers on a substrate and the results show that collection efficiency and pressure drop increase with the

addition of the fiber layer. For 30 minutes of microparticle filtration, there was a collection efficiency of 97.2%. Collection efficiency increase of around 20% for nanoparticle filtration and for t = 0 microparticle filtration. Thus, the addition of a single PAN nanofiber layer positively affected filtration performance, mainly for microparticle evaluation. Thus, Forcespinning equipment could be a promising device for the production of nanofibers for air filtration applications.

4.4. CONCLUSION

This paper study the filtration performance of substrate and PAN nanofiber covered substrate produced by Forcespinning (centrifugal spinning equipment), evaluating the collection efficiency of micro and nanoparticles, and the characteristics of the fiber layer. The fiber layer had a single layer with large fiber diameter dispersion and pore size.

Evaluating filtration performance, the substrate presented more permeable than the covered substrate. The covered substrate was higher pressure drop and collection efficiency than the substrate. For nanoparticle, collection efficiency had an increase of around 20% with the addition of PAN nanofibers. For microparticle collection efficiency, at the begging of the experiment substrate had a collection efficiency of 50.5%, and the covered substrate had 71.0%. After 30 minutes of filtration, the substrate remains in deep filtration, while the PAN fiber layer promoted surface filtration enabled the cake formation, which significantly increased collection efficiency, 97.2%.

5. EVALUATION OF SPUN FIBERS COVERED FILTER MEDIA CONTAINING THYME ESSENTIAL OIL WITH ANTIMICROBIAL PROPERTIES

5.1. INTRODUCTION

Many health problems have been associated with air pollution, furthermore, the bioaerosols have become a huge preoccupation for indoor air quality (World Health Organization, 2017). Bioaerosols are pathogenic or nonpathogenic fungi and bacteria, viruses, pollen, plants piece, for example (Xu *et al.*, 2011). Airborne bioaerosols generally range in size from 1.0 to 5.0 μm (Ghosh, Lal and Srivastava, 2015). Exposure to biological particulate matter has been with health problems like irritation of the respiratory tract and eyes, asthma, rhinitis, bronchitis, rashes on the skin, cancer, diarrhea, headache, hypersensitivity pneumonitis (Douwes *et al.*, 2003; Menetrez *et al.*, 2009). Because of this, strict control is required of the bioaerosols is needed, especially in hospitals, and the food, cosmetics, and pharmaceutical industries (Masotti *et al.*, 2019; Stockwell *et al.*, 2019).

Air filtration has been used to remove bioaerosols. Filter media are relatively simple and less expensive than other collection techniques (Ghosh, Lal and Srivastava, 2015). Therefore, some filter media may be colonized by bacteria and fungi (Maus, Goppelsröder and Umhauer, 2001; Noris, Siegel and Kinney, 2011). An alternative to this challenge is the manufacture of filter media impregnated with an antimicrobial material. Therefore, some antimicrobial agents have been used for filtration application as silver (Lala *et al.*, 2007), chitosan (Desai *et al.*, 2009), fiberglass-acrylic (Cecchini *et al.*, 2004), and some natural alternatives have been taken into consideration as *Sophora flavescens* (Choi *et al.*, 2015), propolis and grapefruit seed extracts (Woo *et al.*, 2015).

Taking into account natural alternatives, the essential oils have been used to combat bacteria, fungi, and viruses since antiquity (Hammer, Carson and Riley, 1999). Some essential oil commonly used for antimicrobial activity application were thyme (Niu *et al.*, 2016), cumin (Alizadeh Behbahani, Noshad

and Falah, 2019), oregano (Zhou *et al.*, 2018), ginger (Silva *et al.*, 2018), cinnamon (Jiang *et al.*, 2019), clove (Radünz *et al.*, 2019), garlic and onion (Benkeblia, 2004). Essential oil is used as an antimicrobial agent for many purposes such as biofilm (Kavanaugh and Ribbeck, 2012), food application (Gutierrez, Barry-Ryan and Bourke, 2008; Sallam, Ishioroshi and Samejima, 2004), wound dressing (Liakos *et al.*, 2014), and medicine (Vuuren, Van, Suliman and Viljoen, 2009). Recently, the studies have been incorporated the essential oil into spun fibers. Mori *et al.* (2015) evaluated the effect of inclusion of candeia essential oil on the properties of polylactic acid mats obtained by electrospinning. Rieger and Schiffman (2014) added cinnamaldehyde in chitosan/poly(ethylene oxide) solution and spun into mats by electrospinning. The cinnamaldehyde promoted high inactivation rates against *Escherichia coli* and *Pseudomonas aeruginosa*. Balasubramanian and Kodam (2014) spun PAN-lavender oil nanofibers by electrospinning with the halo of inhibition unchanged for 30 days for *Staphylococcus aureus* and *Klebsiella pneumoniae* bacteria. Zhang *et al.* (2017) investigated mechanical and antimicrobial properties of polylactic acid fibers containing *Melaleuca alternifolia* and *Leptospermum scoparium* essential oil. The fiber produced halo of inhibition for *Staphylococcus epidermidis*. As could be seen, essential oils have been used as a microbial agent in several applications and have been successfully added to spun fiber. In filter media, the use of metals as antimicrobial agents has stood out. However, the metals are toxic when inhaled, in case of the metals loosen of filter media and re-entrance to the air stream. Thus, the addition of essential oil to the fiber covered filter medium can be a promising choice against bioaerosols.

Among the various methods of fiber production as electrospinning (Deitzel *et al.*, 2001), pressurized gyration (Mahalingam and Edirisinghe, 2013), melt blowing (Ward, 2005), and solution blow spinning (Medeiros *et al.*, 2009), the centrifugal spinning technique has been highlighted. Because, the centrifugal spinning method allows a wide range of materials, and high-concentration solutions, no dependent on solution conductivity, having high productivity, low costs, large-scale production, eco-friendly process, and equipment easy to implement (Lu *et al.*, 2013; Padron *et al.*, 2013; Sarkar *et al.*,

2010).

Therefore, the aim of this study was manufactured fiber covered filter media containing essential oil produced by centrifugal spinning with antimicrobial effect. The antimicrobial effect of some essential oils was evaluated. The fiber layer was spun on the substrate producing the fiber covered filter media. The thyme essential oil was incorporated in filter media using two methods: sprayed on the fiber covered filter media and added to the PAN solution on the manufacturing process, producing two filter media modified. The collection efficiency of micro and nanoparticles, pressure drop, and permeability of the filter media were evaluated and the microbial reduction for *Escherichia coli* and *Staphylococcus aureus* bacteria promoted by thyme essential oil added to filter media was verified quantitatively.

5.2. MATERIALS AND METHODS

5.2.1. **Materials**

Polyacrylonitrile (PAN, Mw: 150,000 g/mol, Sigma-Aldrich) and N, N-dimethylformamide (DMF, anhydrous, 99.8%, Sigma-Aldrich) were used to produce the spun fibers. Indian thyme, clove, and oregano essentials oils purchased from Destilaria Bauru and cinnamon essential oil purchased from Terra Flor Aromaterapia were used as an antimicrobial agent. A cellulose fiber filter medium was used as a substrate. Sodium chloride (NaCl, 99%, Sigma-Aldrich) was used to generate nanoparticles and the hydrated lime powder was used as microparticles. Antibacterial tests were done with Gram-negative *Escherichia coli* (ATCC 8739) and Gram-positive *Staphylococcus aureus* (ATCC 6538) from INCQS - FioCruz. Plate Count Agar (PCA) was used to assess bacterial growth and Mueller Hinton Agar was used to Agar well diffusion method, purchased from Oxoid. Phosphate-buffered saline (PBS) was used to do the dilutions of the antimicrobial tests. Tryptone soy broth (TSB) was used as a broth for the growth of bacteria, purchased from Oxoid.

5.2.2. **Methods**

5.2.2.1. Fiber production

The fibers were prepared from solutions of 10 wt % PAN, and 10 wt % PAN plus 5 wt % thyme essential oil, both dissolved in DMF by stirring for 8 hours. Forcespinning (FS) is composed of the spinneret and collector, as shown in Figure 23 (a). The collector chose was the vacuum collection system (VCS). The substrate was fixed on the VCS (Figure 23 b), and the solution was put in the spinneret to spin the fibers. The solution flowed through the needles by centrifugal forces. After that, the solution jets were elongated because of the resistance promoted by the air (Padron *et al.*, 2013). Finally, the fibers were deposited on the substrate, producing the filter medium.

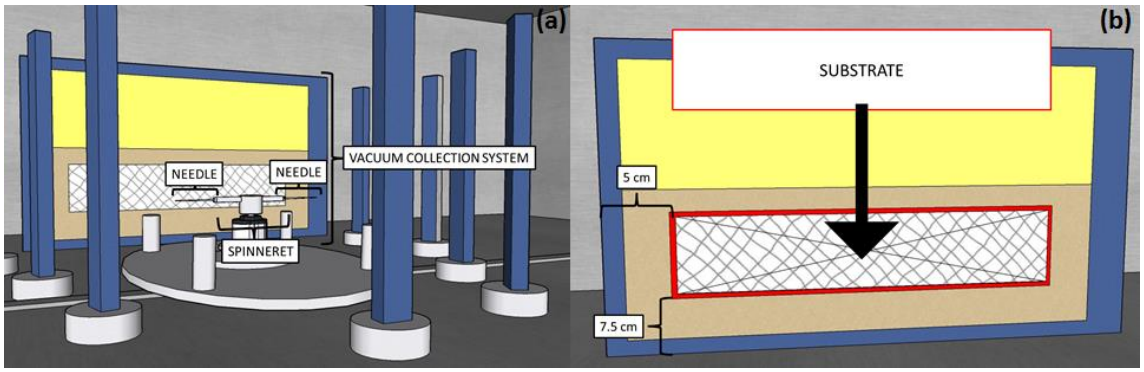

Figure 23. (a) Schematic illustration of the Forcespinning equipment and (b) vacuum collection system.

The operational conditions of Forcespining equipment were 30-gauge half-inch needles, 10 cm needle-collector distance, 8000 rpm rotation speed, 480 s collection time, and 50% VCS power. These operating conditions were based on the study by Lu *et al.* (2013). The covered filter medium produced from the solution of 10 wt. % PAN plus 5 wt. % thyme essential oil was named 5THY. The covered filter medium produced from the solution of 10 wt. % PAN had another process. Thyme essential oil was sprayed on the filter media from 5 cm distance, producing a filter medium with 3.1 mg of thyme essential oil per square centimeter. This filter medium was named THY.

5.2.2.2. Characterization of the fiber layer

The fibers layers were characterized by an analysis of images. The images were acquired by scanning electron microscopy (SEM), using Philip XL-30 FEG instrument, with 2000x of magnification. The fiber diameter was measured on Image Pro-Plus 7.0 using the Bortolassi, Guerra and Aguiar (2017) method.

5.2.2.3. Filtration test

The nanoparticles collection efficiency, permeability, and pressure drop of the filter media were measured on the filtration apparatus represent in Figure 24. The filtration apparatus, Figure 24, consisted of the aerosol generator (Model 3079, TSI), filtered air supply (Model 3074B, TSI), diffusion dryer (Model 3062, TSI), krypton-85 charge neutralizer (Model 3054, TSI), filter media apparatus, americium-241 charge neutralizer, flowmeter (Gilmont), and scanning mobility particle sizer (SMPS) composed of electrostatic classifier (Model 3080, TSI), differential mobility analyzer, and particle counter (Model 3776, TSI).

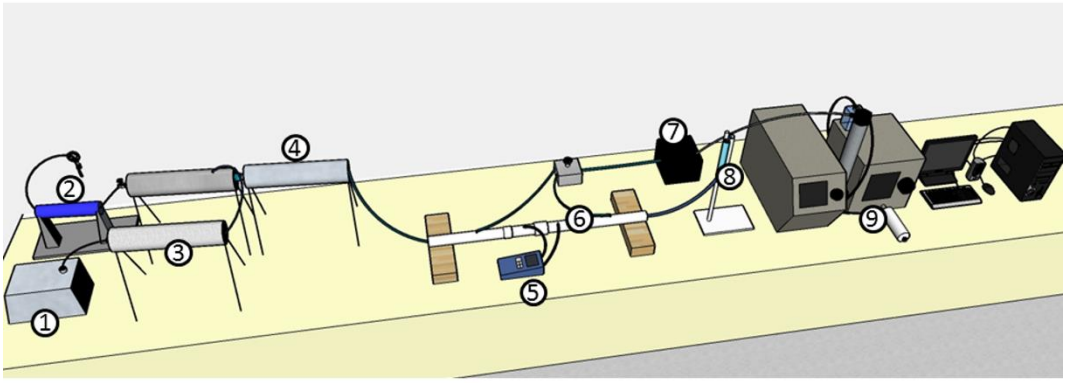

1 atomizer aerossol generator (TSI 3079)
2 filtered air supply (TSI 3074 B)
3 diffusion dryer (TSI 3062)
4 krypton 85 neutralizer (TSI 3054)
5 digital manometer (TSI 9555 P)
6 filter media apparatus
7 americium 241 neutralizer
8 flowmeter shielded tube size 12 (Gilmont)
9 scanning mobility particle sizer spectrometer – electrostatic classifier (TSI 3080) and ultrafine condensation particle conter (TSI 3776)

Figure 24. Schematic illustration of the filtration apparatus of nanoparticles.

The microparticles collection efficiency was measured on the filtration apparatus represent in Figure 25. This filtration has the particle feeder (model 3433, TSI), diluter (model 3302A, TSI), aerodynamic particle sizer spectrometer (model 3320, TSI), flowmeter (Gilmont), and pump.

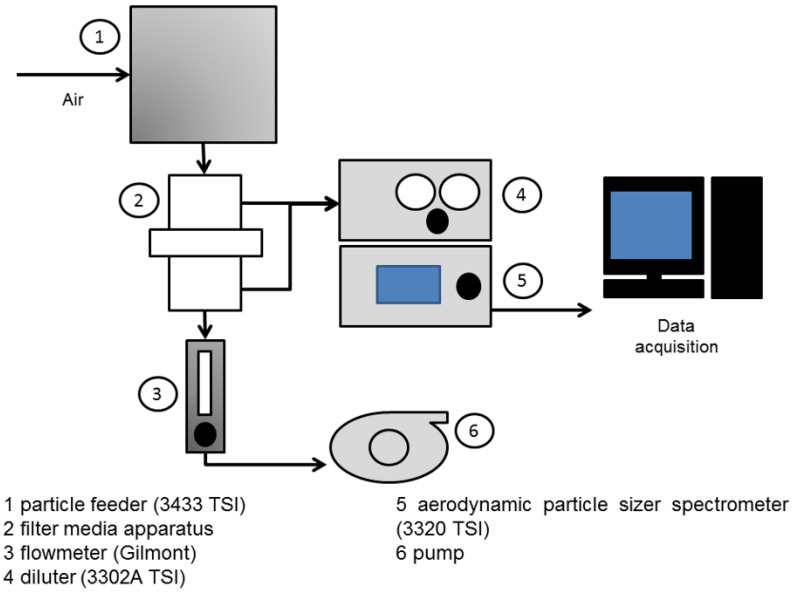

Figure 25. Schematic illustration of the filtration apparatus of microparticles.

5.2.2.3.1. Pressure drop

The pressure drop was measured using a digital manometer VelociCalc, Model 3A-181WP09, TSI Company, as described by Barros, Tanabe and Aguiar (2016).

5.2.2.3.2. Permeability

Permeability constant (k) of each filter media was obtained using Darcy's (Hinds, 1999), Equation 25:

$$\frac{\Delta P}{L} = \frac{\mu\, v_L}{k} \qquad (25)$$

where ΔP is the pressure drop (Pa), L is the thickness of the filter media (cm), μ is the fluid viscosity (Pa s), v_L is the face velocity (cm/s), and k is the permeability constant of the filter media (cm^2).

Permeability was calculated for face velocity that ranged from 0.3 to 6.4 cm/s. The pressure drop was measured at each point. The thickness of the filter media was measured on optical microscope Model BX60, Olympus Company. The viscosity (μ) was considered the air viscosity of 1.74 10^{-7} Pa s.

5.2.2.3.3. Collection efficiency

The collection efficiency was measured for nano and microparticle. The collection efficiency was calculated by Equation 26:

$$E = \frac{C_0 - C_1}{C_0} x100 \quad (26)$$

where E is the collection efficiency (%), C_0 is the particle concentration before the filter media (dW/dlogDp), and C_1 is the particle concentration after the filter media (dW/dlogDp).

The microparticles collection efficiency was evaluated for particle size ranged from 0.54 to 10.37 µm. The microparticles were hydrated lime powder; the particle density is 2.77 g/cm^3. The particle concentrations before and after the filter media were determined in APS. The filtration area was 17.6 cm² and the superficial face velocity was 4.8 cm/s. This powder was chosen especially because the airborne bacteria and fungi have a medium size of 5.11 µm and 4.10 µm, respectively, according to Gao *et al.* (2016).

The nanoparticle collection efficiency was evaluated for particle size ranged from 10.6 to 495.8 nm to assess the filtration performance of particles smaller than bioaerosols. These small particles are linked to serious health problems as warned by the World Health Organization (World Health Organization, 2006). These particles were generated through the aerosol generator from a solution of 1.0 g/L NaCl. The particle concentrations before and after the filter media were determined using the SMPS 15 minutes after the start of the test. The filtration area was 5.2 cm² and the face velocity was 4.8 cm/s.

5.2.2.4. Antimicrobial test

The antibacterial tests were done with Gram-negative *Escherichia coli* bacterium and Gram-positive *Staphylococcus aureus* bacterium. For each experiment, a bacterial suspension was prepared. An aliquot of the bacterial suspension was prepared, inoculated into TBS, and incubated at 37 ºC overnight. Then, the bacterial suspension cultivated was centrifugate and the culture medium was discarded to remove nutrients. The bacterial suspension was diluted in TBS to obtain a bacterial concentration of 10^8 CFU/mL according to absorbance measured at 600 nm for the halo of inhibition and 10^6 CFU/mL for the quantitative test. The tests were performed in triplicate.

5.2.2.4.1. Agar well diffusion method

The first step was performing the halo of inhibition test to choose the essential oil used as an antimicrobial agent. The essential oils used were from cinnamon, clove, oregano, and thyme. These tests were performed according to Jorgensen and Turnidge (2015). For this test, the PCA plates were perforated to have 4 equidistant holes. After that, the plates were inoculated with *Escherichia coli* and *Staphylococcus aureus* bacteria. Then, 25 µl of each oil was deposited in the wells. The plates were incubated at 37 ° C for 24 hours. After this period, the diameter of the halo of inhibition around each well was measured.

5.2.2.4.2. Quantitative test

The quantitative test was done to quantify the reduction of bacteria promoted by the antimicrobial agent. This test was an adaptation by Bortolassi *et al.* (2019). The test were asses in the substrate, 5THY, and THY. The samples were standardized with 2.25 cm^2. The samples were disinfected by ultraviolet radiation for 30 min. To perform the test, each sample and 1000 µL of the bacterial suspension was put into a falcon tube. The falcon tubes were incubated for 5 h at room temperature and stirring (160 rpm). The bacterial concentrations were monitored by the plaque assay method. Control falcon tubes were performed simultaneously.

For the plaque assay method, 100 µl of each sample solution was spread in PCA plate and incubated at 37 °C for 24 hours. After that, the colonies were counted and the concentrations of bacteria in the plate were calculated as the average of the number of colonies divided by the volumes inoculated on the plate multiply by the dilution factor. The counts were used to calculate the surviving number of bacteria. The antibacterial effect is the reduction of bacterial colonies, which can be calculated by Equation 27:

$$R = \frac{(B_0 - B_1)}{B_0} x100 \quad (27)$$

where R is the reduction (%), B_0 the number of bacterial colonies from the sample without thyme essential oil (CFU), and B_1 the number of bacterial colonies from the sample with thyme essential oil (CFU).

5.3. RESULTS AND DISCUSSION

5.3.1. **Characterization of the fiber layer**

The fiber diameter was measured by Image-Pro Plus software through SEM images of the fiber layer. The fiber diameter of the filter medium named 5THY was 1544 ± 101 nm, and THY was 821 ± 73 nm. The fiber layer of 5THY and THY can be seen in Figure 26 (a) and (b), respectively.

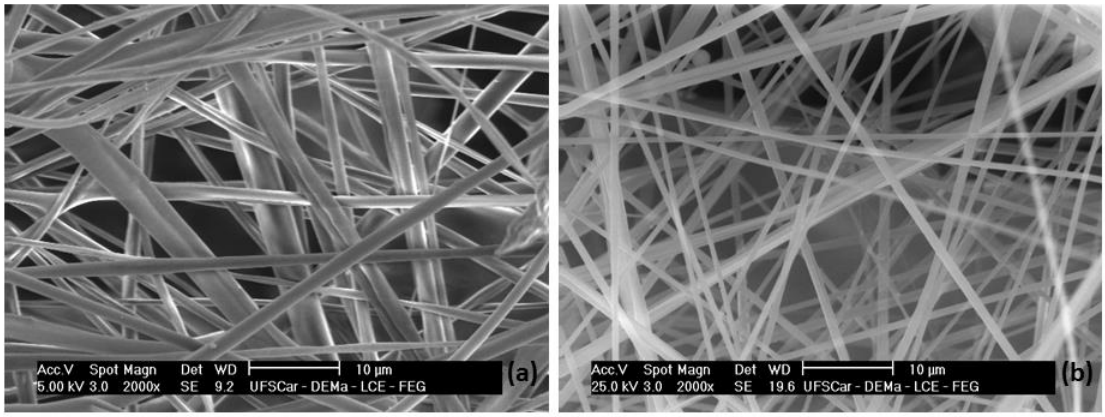

Figure 26. SEM image of fiber layer with 5000x of magnification of (a) 5THY and (b) THY.

The addition of thyme oil to the PAN solution promoted the increase of the fiber diameter. Mori *et al.* (2015) and Zhang *et al.* (2017) also found that the addition of essential oil to the polymeric solution increased the fiber diameter compared to fiber produced without the essential oil. Fiber diameter is affected by the solution viscosity (Padron *et al.*, 2013). The increase in solution viscosity leads to large fiber diameters (Lu *et al.*, 2013). The interaction between PAN and the essential oil may have been affected by the solution viscosity and consequently the fiber diameter. Oliveira *et al.* (2013) reported that the rheology of the polymer solutions may change due to the type and intensity of the interactions between the components of the solution.

The filter medium 5THY had the distribution of fiber diameter that ranged from 73 to 4487 nm and THY ranged from 7 to 2143 nm. This indicates that THY had fibers thinner than 5THY, as can be seen in Figure 27 (a) and (b). These figures show the distributions of fiber diameter of filter medium 5THY and THY, respectively.

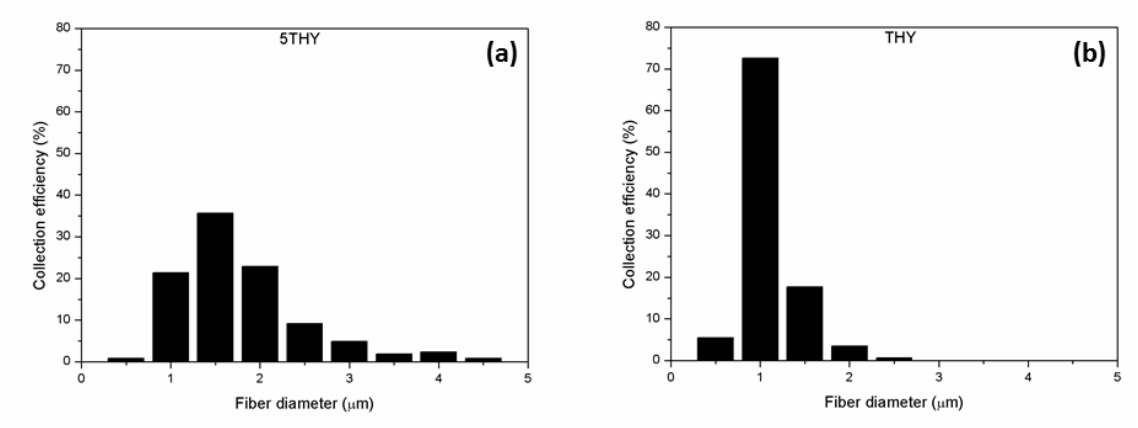

Figure 27. The fiber diameter distribution of the filter medium (a) 5THY and (b) THY.

5.3.2. **Filtration test**

The filtration test that is collection efficiency, pressure drop, and permeability were asses in the substrate, 5THY, and THY can be seen in Table 10. The covered filter media had a higher pressure drop than the substrate. This behavior was expected because a fiber layer was added to the substrate in both cases. However, THY had higher pressure drop than 5THY, it occurs because THY had thinner fibers than 5THY, Figure 27 (a) and (b). Brown (1993) asserted that the pressure drop increases significantly when the fiber diameter decreases. The pressure drop values may also be justified by permeability. THY had smaller permeability than 5THY and the substrate, in which the values increase respectively. Thus, substrate, 5THY, and THY provided greater difficulty for the air to pass through the filter media, respectively. Figure 28 showed the pressure drop/thickness against the face velocity of the substrate, 5THY, and THY. The linear regression of the covered filter media (THY and 5THY) had higher steepest curves than the substrate.

Table 10. Filtration tests of the substrate, 5THY, and THY.

	Substrate	**5THY**	**THY**
Nanoparticle collection efficiency (%)	28 ± 7	45 ± 7	58 ± 5
Microparticle collection efficiency (%)	74 ± 5	87 ± 4	99 ± 0
Pressure drop (Pa)	7.9 ± 0.2	15.7 ± 2.6	32.8 ± 4.3
Permeability (m^2)	$7.4\ 10^{-7} \pm 0.5\ 10^{-7}$	$3.8\ 10^{-7} \pm 1.0\ 10^{-7}$	$1.8\ 10^{-7} \pm 0.3\ 10^{-7}$

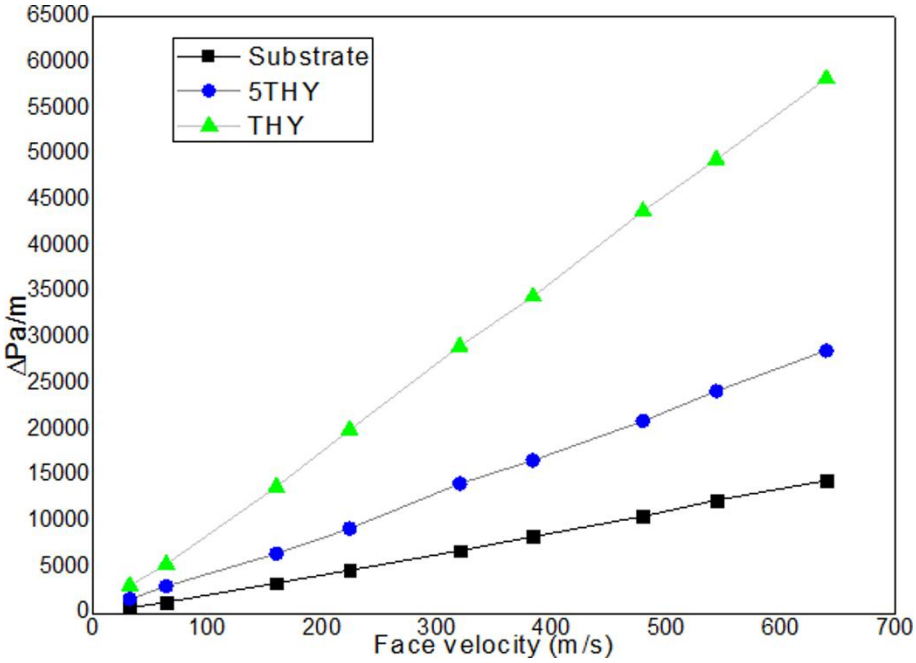

Figure 28. The linear regression of pressure drop/thickness against face velocity of the substrate, 5THY, and THY.

The collection efficiency of nano and microparticle can be seen in Figure 29 (a) and (b), respectively. The collection efficiency of nanoparticle was also evaluated. Figure 29 (a) showed that the nanoparticle collection efficiency of THY was 58 ± 5 %, 5THY of 45 ± 7 %, and the substrate of 28 ± 7 %. THY had the highest collection efficiency in both cases because THY had the smallest fiber diameter. Balgis *et al.* (2015) and Yun *et al.* (2010) demonstrated that the smaller average fiber diameter can significantly improve the collection efficiency in the filter media. The microparticle ranged from 0.54 to 10.37 µm. The substrate had microparticle collection efficiency of 74 ± 5 %, 5THY of 87 ± 4 %, and THY of 99 ± 0 %, as can be seen in Figure 29 (b). Salussoglia, Tanabe and Aguiar (2019) realized that the addition of fiber layer promoted an increase in microparticle collection efficiency and pressure drop because the fiber layer promoted surface filtration enabled the cake formation.

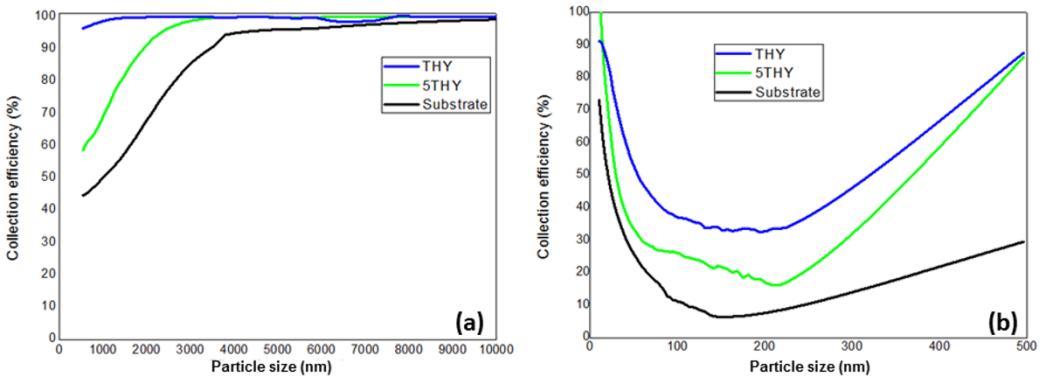

Figure 29. The collection efficiency of (a) nano and (b) microparticle.

5.3.3. **Antimicrobial test**

5.3.3.1. Agar well diffusion method

The agar well diffusion method was performed with cinnamon, clove, oregano, and thyme essential oils. These tests were done with *Escherichia coli* and *Staphylococcus aureus* bacteria. The diameter of the halo of inhibition for thyme essential oil was 70.5 ± 0.5 mm for *Staphylococcus aureus* and 23.2 ± 1.8 mm for *Escherichia coli*, cinnamon was 26.2 ± 0.7 and 25.5 ± 0.5 mm, clove was 20.5 ± 0.8 and 15.8 ± 0.1 mm, and oregano 41.3 ± 3.1 and 17.0 ± 0.6 mm, respectively for each bacteria. Thyme essential oil had the best performance and it was chosen as an antimicrobial agent. Khan, Shafee and Asif (2017) obtained the halo of inhibition of 31 for *Escherichia coli* and 25 mm for *Staphylococcus* of Pakistani variety of thyme essential oil with 15 µL. Walentowska and Foksowicz-Flaczyk (2013) found the antimicrobial effect on the halo of inhibition test for 8% thyme essential oil added to the protection of natural textiles. There was no count for *Corynebacterium xerosis*, *Micrococcus luteus*, and *Staphyloccocus haemolyticus* and the halo of inhibition exceeded 5 mm for *Bacillus licheniformis*, *Staphyloccocus aureus*, *Escherichia coli*, *Klebsiella pneumoniae*, and *Pseudomonas aeruginosa*

5.3.3.2. Quantitative test

The quantitative tests were performed on the substrate, THY, and 5THY for *Escherichia coli* and *Staphylococcus aureus* bacteria. The bacterial counts logarithm of the control was performed in the substrate, 5THY, and THY for *Escherichia coli* and *Staphylococcus aureus* bacteria, as can be seen in Figure

30. The logarithm CFU/mL of control of substrate, 5THY, and THY for *Staphylococcus aureus* were 5.9, 3.4, 2.4 and 1 and for *Escherichia coli* were 6.3, 5.6, 5.5 and 1, respectively. Thus, the substrate had an antimicrobial effect for *Staphylococcus aureus* and *Escherichia coli*, especially for *Staphylococcus aureus*. Lin, Zhu and Cui (2018) developed electrospun thyme essential oil/gelatin nanofibers for active packaging against *Campylobacter jejuni* in chicken and the population of the bacteria treated with free thyme essential oil decreased by 2.2 log CFU/mL in 24 h.

The 5THY filter medium had a reduction of 15.5% and 89.0% for *Escherichia coli* and *Staphylococcus aureus* bacteria, respectively. The THY filter medium had no count of bacteria in the plates, that is the detection limit is less than 10 CFU/ml; it means 99.999% of reduction. On the 5THY filter medium, the essential oil was added to the fibers before the spin. This may have caused the imprisonment and/or evaporation of the essential oil during the spinning process, and thus, decreased the bacteria reduction. The THY filter medium has the essential oil on the surface of the fibers, available, facilitating the inhibition of bacteria.

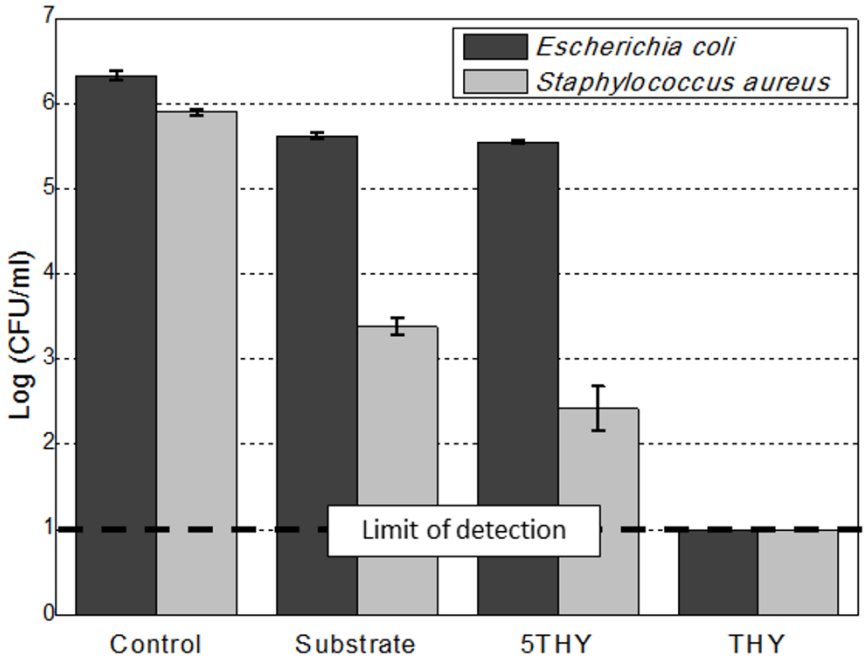

Figure 30. The logarithmic of counted microorganisms for *Escherichia coli* and *Staphylococcus aureus* bacteria of control, substrate, 5THY, THY.

Therefore, the fiber covered filter media impregnated with thyme essential oil proved to be an efficient method against airborne bioaerosols (size ranged from 1 – 5 μm). These filter media captured microparticles efficiently (99%) and still inactivated *Escherichia coli* and *Staphylococcus aureus* bacteria with 99.999% of reduction.

5.4. CONCLUSION

The agar well diffusion method was performed with cinnamon, clove, oregano, and thyme essential oils for *Escherichia coli* and *Staphylococcus aureus* bacteria. Thyme essential oil had the largest halo of inhibition and it was chosen as an antimicrobial agent. The fibers were spun on the substrate for obtaining the filter media 5THY and THY. In 5THY, the thyme essential oil was added to PAN solution, while that, in THY, the thyme essential oil was sprayed on filter media after the manufacturing process. The fibers covered filter media (5THY and THY) showed higher pressure drop and collection efficiency of nano and microparticle and smaller permeability than the substrate. THY had higher collection efficiency than substrate and 5THY, 99% for microparticles and 58% for nanoparticles. By the antimicrobial test, THY had a higher reduction for *Escherichia coli* and *Staphylococcus aureus* than 5THY, resulting in no count of bacteria in the plates. Thus, the THY filter medium performed better, the collection efficiency of microparticles was 99% and Escherichia coli and Staphylococcus aureus bacteria were inactivated with 99.999% of efficiency. Besides, the spun fiber-containing essential oil can be used for many areas such as food, pharmaceuticals, wound dressing, for example.

6. CONCLUSIONS AND SUGGESTIONS FOR FUTURE STUDIES

This study evaluated the characteristic of the fiber layer produced by centrifugal spinning varying the operational conditions of the equipment, solvent and substrate type, and filtration performance of the covered filter media. Besides, the antimicrobial effect of the *Escherichia coli* and *Staphylococcus aureus* bacteria promoted by thyme essential oil added to filter media.

In chapter 2, it was observed that the influence of the vacuum collection system (VCS) as a collector on fibers produced by the centrifugal spinning technique in the filter media type used as the substrate, VCS power, collection time, rotation speed, and needle diameter on the fiber layer characteristics and the filtration performance. As main results, the evaluation of the different types of substrates reported that the combination of the use of a VCS and substrates with different permeability led to the formation of fiber layers with different characteristics in terms of fiber diameter, porosity, and pore size (higher substrate permeability promoted lower porosity of fiber layer). The increase of VCS power promoted an increase in the collection efficiency and pressure drop and a decrease in the porosity and fiber diameter. The collection time had a strong effect on fiber diameter, higher collection time increased the fiber diameter. A comparison of the filtration performances of the filter media without and with a fiber layer showed that the addition of the fiber layer led to increase in the pressure drop and collection efficiency, together with permeability decrease.

In Chapter 3, the fiber diameter, pore area, superficial porosity and filtration performance of substrate covered with PAN fibers produced from DMF and DMSO solutions were compared. Even that the DMF filter medium had smaller fiber diameter and pore size than the DMSO filter medium and close superficial porosity, the collection efficiency had close value. This can indicate that DMSO promoted a stronger and more consistent polarization of PAN than DMF, increasing the collection efficiency of the DMSO filter medium.

In Chapter 4, it was studied the filtration performance of pure substrate and PAN fiber covered substrate produced by centrifugal spinning technique, evaluating the collection efficiency of micro and nanoparticles, and the

characteristics of the fiber layer. The fiber layer had a single layer with large fiber diameter dispersion and pore size. The covered substrate was higher pressure drop and collection efficiency and smaller permeability than the substrate. For nanoparticle, collection efficiency had an increase of around 20% with the addition of PAN fibers. For microparticle collection efficiency, at the begging of the experiment the substrate had a collection efficiency of 50.5%, and the covered substrate had 71.0%. After 30 minutes of filtration, the substrate remains in deep filtration, while the PAN fiber layer promoted surface filtration, which significantly increased collection efficiency, 97.2%.

In Chapter 5, the fibers were manufactured by centrifugal spinning technique under the operational conditions: 30-gauge half-inch needles, 10 cm needle-collector distance, 8000 rpm rotation speed, 480 s collection time, and 50% VCS power. The thyme essential oil was added to PAN solution on 5THY, while that on THY, the thyme essential oil was sprayed after the filter media produced. The fibers covered filter media were higher pressure drop and collection efficiency of nano and microparticle and smaller permeability than the substrate. THY had higher collection efficiency than substrate and 5THY, 99% for microparticles and 58% for nanoparticles. Through the antimicrobial test, THY had a higher reduction for *Escherichia coli* and *Staphylococcus aureus* bacteria than 5THY, resulting in no count of bacteria in the plates.

In this study, the thyme essential oil showed excellent results as an antimicrobial agent and the fiber covered filter media, produced by the centrifugal spinning equipment, showed great filtration performance, especially for microparticles. It is suggested as continuity of this research: to investigate the fiber production by the centrifugal spinning using other solvents, polymers (especially most advantageous polymers in terms of cost such as recycled polymers, nylon, polyethylene terephthalate, polypropylene, and polyethylene), and different operating conditions of the equipment (there are few studies in the literature), to investigate other alternatives of natural antimicrobial agents as isolate compost, and to perform stability tests of the antimicrobial agent added to the filter medium.

7. **APPENDIX**

The appendix shows the difficulties encountered in carrying out this work.

For the production of the PAN solution, the instruments must be extremely dry, the solution is well sealed in the beaker, and also that the same instruments (metal bar, beaker, agitator) are used to maintain standardized viscosity.

It is important to verify the humidity inside the equipment for the solvent evaporation to be constant. Besides, the humidity and temperature room. The fibers were not spun when the humidity in the air was over 35%.

The JIS Z 2801/ISO 22196 methodology was tested and adapted to quantify the reduction of bacteria caused by the sample. However, there was no counting on the Petri dishes, not even in the white test. Thus, it was decided to use the methodology of the Bortolasi et al. (2019), which was also adapted to carry out the tests.

The technical data sheets of some essential oils indicated good results as an antimicrobial agent and for that, some essential oils were tested. However, when using the agar well diffusion method, it was found that some of these essential oils did not obtain good results for *Escherichia coli* and *Staphylococcus aureus* bacteria. For example, the essential oils of turmeric, eucalyptus, copaiba that had the halo of inhibition 0, 0, and 0 cm for *Escherichia coli*, respectively, and the halo of inhibition of 0, 2.41 ± 0.13, and 2.23 ± 0.06 cm for *Staphylococcus aureus*, respectively. These essential oils were refused.

REFERENCES

AGUBRA, V. A. *et al.* ForceSpinning of polyacrylonitrile for mass production of lithium-ion battery separators. **Journal of Applied Polymer Science**, v. 133, n. 1, p. 1–8, 2016.

AKIA, M. *et al.* Antibacterial activity of polymeric nano fiber membranes impregnated with Texas sour orange juice. **European Polymer Journal**, v. 115, n. February, p. 1–5, 2019.

AKTHAR, M.; DEGAGA, B.; AZAM, T. Antimicrobial activity of essential oils extracted from medicinal plants against the pathogenic microorganisms: a review. **Issues in Biological Sciences and Pharmaceutical Research**, 2014.

ALI, B. *et al.* Essential oils used in aromatherapy: A systemic review. **Asian Pacific Journal of Tropical Biomedicine**, v. 5, n. 8, p. 601–611, 2015.

ALIZADEH BEHBAHANI, B.; NOSHAD, M.; FALAH, F. Cumin essential oil: Phytochemical analysis, antimicrobial activity and investigation of its mechanism of action through scanning electron microscopy. **Microbial Pathogenesis**, v. 136, n. August, p. 103716, 2019.

ALOK, K.; RAKESH, T.; SUSHIL, K. Aromatherapy-an alternative health care through essential oils. **Journal of Medicinal and Aromatic Plant Science**, 2000.

BALASUBRAMANIAN, K.; KODAM, K. M. Encapsulation of therapeutic lavender oil in an electrolyte assisted polyacrylonitrile nanofibres for antibacterial applications. **RSC Advances**, v. 4, n. 97, p. 54892–54901, 2014.

BALGIS, R. *et al.* Synthesis and evaluation of straight and bead-free nanofibers for improved aerosol filtration. **Chemical Engineering Science**, v. 137, p. 947–954, 2015.

BARROS, P. M.; TANABE, E. H.; AGUIAR, M. L. Performance of fibrous filters during nanoparticle cake formation. **Separation Science and Technology (Philadelphia)**, 2016.

BENKEBLIA, N. Antimicrobial activity of essential oil extracts of various onions

(Allium cepa) and garlic (Allium sativum). **LWT - Food Science and Technology**, v. 37, n. 2, p. 263–268, 2004.

BHATTACHARYA, R.; REDDY, K. R. C.; MISHRA, A. K. Export strategy of Ayurvedic Products from India. **International Journal of Ayurvedic Medicine**, v. 5, n. 1, p. 125–128, 2014.

BORTOLASSI, A. C. C. *et al.* Efficient nanoparticles removal and bactericidal action of electrospun nano fibers membranes for air filtration. **Materials Science & Engineering C**, v. 102, n. October 2018, p. 718–729, 2019.

BORTOLASSI, A. C. C.; GUERRA, V. G.; AGUIAR, M. L. Characterization and evaluate the efficiency of different filter media in removing nanoparticles. **Separation and Purification Technology**, v. 175, p. 79–86, 2017.

BROWN, C. R. **Air Filtration**. London: Pergamon Press, 1993.

CECCHINI, C. *et al.* Effects of antimicrobial treatment on fiberglass-acrylic filters. **Journal of Applied Microbiology**, v. 97, n. 2, p. 371–377, 2004.

CHANG, K. *et al.* A novel, stretchable, silver-coated polyolefin elastomer nanofiber membrane for strain sensor applications. v. 47928, p. 1–7, 2019.

CHOI, J. *et al.* Herbal Extract Incorporated Nanofiber Fabricated by an Electrospinning Technique and its Application to Antimicrobial Air Filtration. **ACS Applied Materials and Interfaces**, v. 7, n. 45, p. 25313–25320, 2015.

CHOI, W.; KIM, J. Characteristics of Ultrafine Particles in Urban Areas Observed Worldwide and in Korea : Sources and Emissions, Spatial and Temporal Distributions, and Health Effects. v. 28, n. 3, p. 337–355, 2018.

CHUANFANG, Y. Aerosol Filtration Application Using Fibrous Media — An Industrial Perspective. **Chinese Journal of Chemical Engineering**, v. 20, n. 1, p. 1–9, 2012.

CINCINELLI, A.; MARTELLINI, T. Indoor air quality and health. **International Journal of Environmental Research and Public Health**, v. 14, n. 11, 2017.

CLIFT, R.; GRACE, J. R.; WEBER, M. E. **Bubbles, drops and particles**. New

York: Academic Press. p. 360. 1978.

COURY, J. R. **Electrostatic effects in granular bed filtration of gases**. Inglaterra: University of Cambridge, 1983.

DEITZEL, J. *et al.* The effect of processing variables on the morphology of electrospun nanofibers and textiles. **Polymer**, v. 42, n. 1, p. 261–272, 2001.

DESAI, K. *et al.* Nanofibrous chitosan non-wovens for filtration applications. **Polymer**, v. 50, n. 15, p. 3661–3669, 2009.

DONOVAN, R. P. **Fabric filtration for combustion sources : fundamentals and basic technology**. New York: Marcel Dekker Inc, 1985.

DOUWES, J. *et al.* Bioaerosol health effects and exposure assessment: Progress and prospects. **Annals of Occupational Hygiene**, v. 47, n. 3, p. 187–200, 2003.

DULLIEN, F. A. L. **Introduction to Industrial Gas Cleaning**. San Diego: Academic Press, 1989.

EOM, Y.; KIM, B. C. Solubility parameter-based analysis of polyacrylonitrile solutions in N,N-dimethyl formamide and dimethyl sulfoxide. **Polymer**, v. 55, n. 10, p. 2570–2577, 2014.

FANG, Y. *et al.* A comparative parameter study: Controlling fiber diameter and diameter distribution in centrifugal spinning of photocurable monomers. **Polymer (United Kingdom)**, v. 88, p. 102–111, 2016.

FARAG, R. S. *et al.* Antimicrobial activity of some essential oils. **Journal of Food Protection**, v. 52, n. 9, p. 665–667, 1989.

FENG, J. P. *et al.* Characterization of filter media prepared from aligned nano fibers for fine dust screen. v. 48166, p. 1–13, 2019.

FLORES, D. *et al.* Production of carbon fibers through Forcespinning® for use as anode materials in sodium ion batteries. **Materials Science & Engineering B**, v. 236–237, n. December, p. 70–75, 2018.

FRIEDLANDER, S. K.; PASCERI, R. E. Measurements of the Particle Size

Distribution of the Atmospheric Aerosol: I. Introduction and Experimental Methods. **Journal of the Atmospheric Sciences**, 1965.

GAO, M. *et al.* Variation of correlations between factors and culturable airborne bacteria and fungi. **Atmospheric Environment**, v. 128, p. 10–19, 2016.

GHOSH, B.; LAL, H.; SRIVASTAVA, A. Review of bioaerosols in indoor environment with special reference to sampling, analysis and control mechanisms. **Environment International**, v. 85, p. 254–272, 2015.

GIBSON, P.; SCHREUDER-GIBSON, H.; RIVIN, D. Transport properties of porous membranes based on electrospun nanofibers. **Colloids and Surfaces A: Physicochemical and Engineering Aspects**, v. 187, n. 188, p. 469–481, 2001.

GONÇALVES, N. D. *et al.* Encapsulated thyme (Thymus vulgaris) essential oil used as a natural preservative in bakery product. **Food Research International**, v. 96, p. 154–160, 2017.

GOPAL, R. *et al.* Electrospun nanofibrous filtration membrane. **Journal of Membrane Science**, 2006.

GRAFE, T.; GRAHAM, K. Nanofiber Webs from Electrospinning. **Nonwovens in Filtration-Fifth International Conference**, n. March, p. 1–5, 2003.

GUTIERREZ, J.; BARRY-RYAN, C.; BOURKE, P. The antimicrobial efficacy of plant essential oil combinations and interactions with food ingredients. **International Journal of Food Microbiology**, v. 124, n. 1, p. 91–97, 2008.

HAMMER, K. A.; CARSON, C. F.; RILEY, T. V. Antimicrobial activity of essential oils and other plant extracts. **Journal of Applied Microbiology**, v. 86, n. 6, p. 985–990, 1999.

HAYES, R. B. *et al.* PM 2 . 5 air pollution and cause-specific cardiovascular disease mortality. v. 3, p. 1–11, 2019.

HINDS, W. C. **Aerosol technology: Properties, Behavior, and Measurement of Airborne Particles.** [s.l: s.n.].

HOBZOVA, R. *et al.* Poly (D,L-lactide)/polyethylene glycol micro/nanofiber mats as paclitaxel-eluting carriers: preparation and characterization of fibers, in vitro drug release, antiangiogenic activity and tumor recurrence prevention. **Materials Science and Engineering C**, v. 98, n. January, p. 982–993, 2019.

HOTALING, N. **DiameterJ**. Disponível em: <https://imagej.net/DiameterJ>. Acesso em: 27 nov. 2019.

HOTALING, N. A. *et al.* DiameterJ: A validated open source nanofiber diameter measurement tool. **Biomaterials**, v. 61, p. 327–338, 2015.

HUANG, Z. M. *et al.* A review on polymer nanofibers by electrospinning and their applications in nanocomposites. **Composites Science and Technology**, 2003.

HWAN, G. B. *et al.* Synthesis of hybrid carbon nanotube structures coated with Sophora flavescens nanoparticles and their application to antimicrobial air filtration. **Journal of Aerosol Science**, v. 86, p. 44–54, 2015.

JIANG, Y. *et al.* Chemical composition and antimicrobial activity of the essential oil of Rosemary. **Environmental Toxicology and Pharmacology**, 2011.

JIANG, Y. *et al.* Cinnamon Essential Oil Pickering Emulsion Stabilized by Zein-pectin Composite Nanoparticles: Characterization, Antimicrobial Effect and Advantages in Storage Application. **International Journal of Biological Macromolecules**, 2019.

JORGENSEN, J. H.; TURNIDGE, J. D. Susceptibility Test Methods: Dilution and Disk Diffusion Methods. *In*: **Manual clinical microbiology**. 11th editi ed. Washington: ASM Press, 2015. p. 1253–1273.

KAVANAUGH, N. L.; RIBBECK, K. Selected antimicrobial essential oils eradicate pseudomonas spp. And Staphylococcus aureus biofilms. **Applied and Environmental Microbiology**, v. 78, n. 11, p. 4057–4061, 2012.

KHAN, Y. H.; SHAFEE, M.; ASIF, M. Antimicrobial activity of Thyme (Thymus vulgaris) essential oil cultivated in Antimicrobial activity of Thyme (Thymus vulgaris) essential oil cultivated in Quetta, Balochistan, Pakistan. v. 6655, n.

February, p. 105–110, 2017.

KIM, S. O. J. K. D. Cellulose-derived tin-oxide-nanoparticle-embedded carbon fibers as binder-free flexible Li-ion battery anodes. **Cellulose**, v. 26, n. 4, p. 2557–2571, 2019.

KINASHI, K. *et al.* Composite Resin Dosimeters: A New Concept and Design for a Fibrous Color Dosimeter. **Applied Materials & Interfaces**, v. 10, p. 11926–11932, 2018.

KLEPEIS, N. E. *et al.* The National Human Activity Pattern Survey (NHAPS): A resource for assessing exposure to environmental pollutants. **Journal of Exposure Analysis and Environmental Epidemiology**, v. 11, n. 3, p. 231–252, 2001.

KRAUSKOPF, J. *et al.* Short-term exposure to traffic-related air pollution reveals a compound- specific circulating miRNA profile indicating multiple disease risks. **Environment International**, v. 128, n. May, p. 193–200, 2019.

KRIFA, M.; YUAN, W. Morphology and pore size distribution of electrospun and centrifugal forcespun nylon 6 nanofiber membranes. **Textile Research Journal**, 2015.

KUMMER, G. *et al.* Development of Nanofibers Composed of Chitosan / Nylon 6 and Tannin / Nylon 6 for Effective Adsorption of Cr (VI). **Journal of Polymers and the Environment**, v. 26, n. 10, p. 4073–4084, 2018.

L V, D. *et al.* **Green Electrospun Nanofibers and Their Application in Air FiltrationMacromolecular Materials and Engineering**, 2018.

LALA, N. L. *et al.* Fabrication of nanofibers with antimicrobial functionality used as filters: Protection against bacterial contaminants. **Biotechnology and Bioengineering**, v. 97, n. 6, p. 1357–1365, 2007.

LEE, K. W.; LIU, B. Y. H. Theoretical study of aerosol filtration by fibrous filters. **Aerosol Science and Technology**, 1982.

LEE, M. *et al.* Long-term effect of fine particulate matter on hospitalization with dementia. **Environmental Pollution**, v. 254, p. 112926, 2019.

LEUNG, W. W.; CHOY, H. Transition from depth to surface filtration for a low-skin effect filter subject to continuous loading of nano-aerosols. **Separation and Purification Technology**, v. 190, n. June 2017, p. 202–210, 2018.

LEUNG, W. W. F.; HAU, C. W. Y.; CHOY, H. F. Microfiber-nanofiber composite filter for high-efficiency and low pressure drop under nano-aerosol loading. **Separation and Purification Technology**, v. 206, n. February, p. 26–38, 2018.

LI, J. *et al.* Needleless electrospun nanofibers used for filtration of small particles. **Express Polymer Letters**, v. 7, n. 8, p. 683–689, 2013.

LI, P. *et al.* Air filtration in the free molecular flow regime: A review of high-efficiency particulate air filters based on Carbon Nanotubes. **Small**, v. 10, n. 22, p. 4553–4561, 2014.

LIAKOS, I. *et al.* All-natural composite wound dressing films of essential oils encapsulated in sodium alginate with antimicrobial properties. **International Journal of Pharmaceutics**, v. 463, n. 2, p. 137–145, 2014.

LIAN, H. *et al.* Effect of the added polysaccharide on the release of thyme essential oil and structure properties of chitosan based film. **Food Packaging and Shelf Life**, v. 23, n. 61, p. 100467, 2020.

LIN, L.; ZHU, Y.; CUI, H. Electrospun thyme essential oil/gelatin nanofibers for active packaging against Campylobacter jejuni in chicken. **Lwt**, v. 97, n. August, p. 711–718, 2018.

LIU, B. Y. H.; RUBOW, K. L. **Efficiency, pressure drop and figure of merit of high efficiency fibrous and membrane filter media**Nice: Proceedings of the 5th World Filtration Congress, 1990

LIU, C. *et al.* Transparent air filter for high-efficiency PM2.5 capture. **Nature communications**, v. 6, p. 6205, 2015.

LU, Y. *et al.* Parameter study and characterization for polyacrylonitrile nanofibers fabricated via centrifugal spinning process. **European Polymer Journal**, v. 49, n. 12, p. 3834–3845, 2013.

LUKÁŠOVÁ, V. *et al.* Materials Science & Engineering C Needleless

electrospun and centrifugal spun poly- ε -caprolactone scaffolds as a carrier for platelets in tissue engineering applications : A comparative study with hMSCs. **Materials Science & Engineering C**, v. 97, n. December 2018, p. 567–575, 2019.

MADUNA, L.; PATNAIK, A. Textiles in air filtration. **Textile Progress**, v. 49, n. 4, p. 173–247, 2017.

MAHALINGAM, S.; EDIRISINGHE, M. Forming of polymer nanofibers by a pressurised gyration process. **Macromolecular Rapid Communications**, v. 34, n. 14, p. 1134–1139, 2013.

MAMIDI, N.; ROMO, I. L.; BARRERA, E. V.; *et al.* High throughput fabrication of curcumin embedded gelatin-polylactic acid forcespun fiber-aligned scaffolds for the controlled release of curcumin. **MRS Communications**, v. 8, n. 4, p. 1395–1403, 2019.

MAMIDI, N.; ROMO, I. L.; GUTIÉRREZ, H. L.; *et al.* Development of forcespun fiber-aligned scaffolds from gelatin – zein composites for potential use in tissue engineering and drug release. **MRS Communications**, v. 8, n. 3, p. 885–892, 2019.

MANDAL, J.; BRANDL, H. Bioaerosols in Indoor Environment - A Review with Special Reference to Residential and Occupational Locations. **The Open Environmental & Biological Monitoring Journal**, 2011.

MASOTTI, F. *et al.* Airborne contamination in the food industry: An update on monitoring and disinfection techniques of air. **Trends in Food Science and Technology**, v. 90, n. June, p. 147–156, 2019.

MAUS, R.; GOPPELSRÖDER, A.; UMHAUER, H. Survival of bacterial and mold spores in air filter media. **Atmospheric Environment**, v. 35, n. 1, p. 105–113, 2001.

MEDEIROS, E. S. *et al.* Solution blow spinning: A new method to produce micro- and nanofibers from polymer solutions. **Journal of Applied Polymer Science**, 2009.

MENETREZ, M. Y. *et al.* An evaluation of indoor and outdoor biological particulate matter. **Atmospheric Environment**, v. 43, n. 34, p. 5476–5483, 2009.

MISSAU, J. *et al.* Purification of crude wax using a filter medium modified with a nanofiber coating. **Chemical Engineering Research and Design**, v. 136, p. 734–743, 2018.

MORI, C. L. S. D. O. *et al.* Nanostructured polylactic Acid/candeia essential oil mats obtained by electrospinning. **Journal of Nanomaterials**, v. 2015, 2015.

NICOSIA, A. *et al.* Cellulose acetate nano fi ber electrospun on nylon substrate as novel composite matrix for efficient, heat-resistant, air filters. v. 153, p. 284–294, 2016.

NIU, F. *et al.* Physical and antimicrobial properties of thyme oil emulsions stabilized by ovalbumin and gum Arabic. **Food Chemistry**, v. 212, p. 138–145, 2016.

NIU, X. *et al.* Rosin modified cellulose nanofiber as a reinforcing and co-antimicrobial agents in polylactic acid/chitosan composite film for food packaging. **Carbohydrate Polymers**, v. 183, n. October 2017, p. 102–109, 2018.

NORIS, F.; SIEGEL, J. A.; KINNEY, K. A. Evaluation of HVAC filters as a sampling mechanism for indoor microbial communities. **Atmospheric Environment**, v. 45, n. 2, p. 338–346, 2011.

O'HAIRE, T. *et al.* Influence of nanotube dispersion and spinning conditions on nanofibre nanocomposites of polypropylene and multi-walled carbon nanotubes produced through ForcespinningTM. **Journal of Thermoplastic Composite Materials**, v. 27, n. 2, p. 205–214, 2013.

OLIVEIRA, J. E. *et al.* Development of poly (lactic acid) nanostructured membranes for the controlled delivery of progesterone to livestock animals. **Materials Science and Engineering C**, v. 33, n. 2, p. 844–849, 2013.

PADRON, S. *et al.* Experimental study of nanofiber production through

forcespinning. **Journal of Applied Physics**, v. 113, n. 2, 2013.

PAYEN, J. *et al.* Influence of fiber diameter, fiber combinations and solid volume fraction on air filtration properties in nonwovens. **Textile Research Journal**, v. 82, n. 19, p. 1948–1959, 2012.

PEREZ-PUYANA, V. M. *et al.* Highly porous protein-based 3D scaffolds with different collagen concentrates for potential application in tissue engineering. **JOURNAL OF APPLIED POLYMER SCIENCE**, v. 47954, p. 1–10, 2019.

RADMANESH, E. *et al.* Cerebral ischemic attack, epilepsy and hospital admitted patients with types of headaches attributed to PM 10 mass concentration in Abadan, Iran. **Aeolian Research**, v. 41, n. December 2017, p. 100541, 2019.

RADÜNZ, M. *et al.* Antimicrobial and antioxidant activity of unencapsulated and encapsulated clove (Syzygium aromaticum, L.) essential oil. **Food Chemistry**, v. 276, p. 180–186, 2019.

RANZ, W. E.; WONG, J. B. Jet impactors for determining the particle-size distributions of aerosols. **Archives of Industrial Hygiene and Occupational Medicine**, v. 5, p. 464–477, 1952.

RIEGER, K. A.; SCHIFFMAN, J. D. Electrospinning an essential oil: Cinnamaldehyde enhances the antimicrobial efficacy of chitosan/poly(ethylene oxide) nanofibers. **Carbohydrate Polymers**, v. 113, p. 561–568, 2014.

ROSTAMIAN, R.; FIROUZZARE, M.; IRANDOUST, M. Preparation and neutralization of forcespun chitosan nano fibers from shrimp shell waste and study on its uranium adsorption in aqueous media. **Reactive and Functional Polymers**, v. 143, n. July, p. 104335, 2019.

ROTHWELL, E. Fabric dust filtration: principles and practice. **Filtration and Separation**, p. 471–475, 1980.

Safety Data Sheet - DMF. Disponível em: <https://www.sigmaaldrich.com/MSDS/MSDS/DisplayMSDSPage.do?country=BR&language=pt&productNumber=319937&brand=SIGALD&PageToGoToURL=

https%3A%2F%2Fwww.sigmaaldrich.com%2Fcatalog%2Fproduct%2Fsigald%2F319937%3Flang%3Dpt>. Acesso em: 19 mar. 2019.

Safety Data Sheet - DMSO. Disponível em: <https://www.sigmaaldrich.com/MSDS/MSDS/DisplayMSDSPage.do?country=BR&language=pt&productNumber=D2650&brand=SIGMA&PageToGoToURL=https%3A%2F%2Fwww.sigmaaldrich.com%2Fcatalog%2Fproduct%2Fsigma%2Fd2650%3Flang%3Dpt>. Acesso em: 19 mar. 2019.

SALLAM, K. I.; ISHIOROSHI, M.; SAMEJIMA, K. Antioxidant and antimicrobial effects of garlic in chicken sausage. **LWT - Food Science and Technology**, v. 37, n. 8, p. 849–855, 2004.

SALUSSOGLIA, A. I. P.; TANABE, E. H.; AGUIAR, M. L. Characterization and micro and nanoparticles filtration evaluation of pan nanofibers produced by centrifugal spinning. **Enciclopédia Biosfera**, v. 16, n. 30, p. 103–112, 2019.

SAMBAER, W.; ZATLOUKAL, M.; KIMMER, D. 3D modeling of filtration process via polyurethane nanofiber based nonwoven filters prepared by electrospinning process. **Chemical Engineering Science**, v. 66, n. 4, p. 613–623, 2011.

SARKAR, K. *et al.* Electrospinning to Forcespinning. **Materials Today**, v. 13, n. 11, p. 12–14, 2010.

SENTHIL, K.; PUNITHA, V. An Overview of Nonwoven Product Development and Modelling of Their Properties. **Journal of Textile Science & Engineering**, 2017.

SILVA, F. T. DA *et al.* Action of ginger essential oil (Zingiber officinale) encapsulated in proteins ultrafine fibers on the antimicrobial control in situ. **International Journal of Biological Macromolecules**, v. 118, p. 107–115, 2018.

STOCKWELL, R. E. *et al.* Indoor hospital air and the impact of ventilation on bioaerosols: a systematic review. **Journal of Hospital Infection**, v. 103, n. 2, p. 175–184, 2019.

TIEN, C.; RAMARAO, B. V. **Granular Filtration of Aerosols and Hydrosols**.

2007.

TSI. **Mechanisms of filtration for high efficiency fibrous filters, Application Note ITI041**. 2012.

VALDEZ, M. *et al.* Sensors and Actuators B : Chemical ForceSpun polydiacetylene nano fibers as colorimetric sensor for food spoilage detection. **Sensors & Actuators: B. Chemical**, v. 297, n. June, p. 126734, 2019.

VUUREN, S. F. VAN; SULIMAN, S.; VILJOEN, A. M. The antimicrobial activity of four commercial essential oils in combination with conventional antimicrobials. **Letters in Applied Microbiology**, v. 48, n. 4, p. 440–446, 2009.

WALENTOWSKA, J.; FOKSOWICZ-FLACZYK, J. Thyme essential oil for antimicrobial protection of natural textiles. **International Biodeterioration and Biodegradation**, v. 84, p. 407–411, 2013.

WALTON, E. L. Tainted air : The link between pollution and Alzheimer ' s disease. **Biomedical Journal**, v. 41, n. 3, p. 137–140, 2018.

WANG, J.; KIM, S. C.; PUI, D. Y. H. Investigation of the figure of merit for filters with a single nanofiber layer on a substrate. **Journal of Aerosol Science**, v. 39, n. 4, p. 323–334, 2008.

WARD, G. Nanofibres: Media at the nanoscale. **Filtration and Separation**, v. 42, n. 7, p. 22–24, 2005.

WILLEKE, K.; BARON, P. A. **Aerosol Measurementet: principles, techniques, and applications.** New York: Van Nostrand Reinhold, 1993.

WILLEKE, K.; BARON, P. A. **Aerossol Measurement: principles, techniques and applications**. New York: Van Nostrand Reinhold, 1993.

WOO, C. G. *et al.* Treatment of Air Filters Using the Antimicrobial Natural Products Propolis and Grapefruit Seed Extract for Deactivation of Bioaerosols. **Aerosol Science and Technology**, v. 49, n. 8, p. 611–619, 2015.

WORLD HEALTH ORGANIZATION. WHO Air quality guidelines for particulate matter, ozone, nitrogen dioxide and sulfur dioxide: global update 2005:

summary of risk assessment. **Geneva: World Health Organization**, p. 1–22, 2006.

WORLD HEALTH ORGANIZATION. **Evolution of WHO air quality guidelines**. p. 39. 2017.

XU, F. *et al.* Large-scale production of a ternary composite nanofiber membrane for wound dressing applications. **Journal of Bioactive and Compatible Polymers**, v. 29, n. 6, p. 646–660, 2014.

XU, Z. *et al.* Bioaerosol science, technology, and engineering: Past, present, and future. **Aerosol Science and Technology**, v. 45, n. 11, p. 1337–1349, 2011.

YIN, G. *et al.* The electrospun polyamide 6 nanofiber membranes used as high efficiency filter materials: Filtration potential, thermal treatment, and their continuous production. **Journal of Applied Polymer Science**, 2013.

YUN, K. M. *et al.* Morphology optimization of polymer nanofiber for applications in aerosol particle filtration. **Separation and Purification Technology**, v. 75, n. 3, p. 340–345, 2010.

ZENG, X. *et al.* Investigating the jet stretch in the wet spinning of PAN fiber. **Journal of Applied Polymer Science**, 2007.

ZHANG, S.; SHIM, W. S.; KIM, J. Design of ultra-fine nonwovens via electrospinning of Nylon 6: Spinning parameters and filtration efficiency. **Materials and Design**, v. 30, n. 9, p. 3659–3666, 2009.

ZHANG, W. *et al.* Electrospinning of polylactic acid fibres containing tea tree and manuka oil. **Reactive and Functional Polymers**, v. 117, n. May, p. 106–111, 2017.

ZHANG, X.; LU, Y. Centrifugal Spinning: An Alternative Approach to Fabricate Nanofibers at High Speed and Low Cost. **Polymer Reviews**, v. 54, n. 4, p. 677–701, 2014.

ZHOU, Y. *et al.* Preparation and antimicrobial activity of oregano essential oil Pickering emulsion stabilized by cellulose nanocrystals. **International Journal**

of Biological Macromolecules, v. 112, p. 7–13, 2018.

ZHU, M. *et al.* Electrospun Nanofibers Membranes for Effective Air Filtration. **Macromolecular Materials and Engineering**, v. 1600353, p. 1600353, 2016.

ZHU, M. *et al.* Green electrospun and crosslinked poly(vinyl alcohol)/poly(acrylic acid) composite membranes for antibacterial effective air filtration. **Journal of Colloid and Interface Science**, v. 511, p. 411–423, 2018.